DOKUZ EYLÜL UNIVERSITY

GRADUATE SCHOOL OF NATURAL AND APPLIED SCIENCES

SEAWATER EFFECT ON BEHAVIORS OF IMPACT AND AXIAL COMPRESSION-AFTER IMPACT OF COMPOSITE PIPES

by

Mehmet Emin DENİZ

September, 2011

İZMİR

SEAWATER EFFECT ON BEHAVIORS OF IMPACT AND AXIAL COMPRESSION-AFTER IMPACT OF COMPOSITE PIPES

A Thesis Submitted to the
Graduate School of Natural and Applied Sciences of Dokuz Eylül University
In Partial Fulfillment of the Requirements for the Degree of Doctor of Philosophy in Mechanical Engineering, Mechanic Program

by
Mehmet Emin DENİZ

September, 2011
İZMİR

Ph.D. THESIS EXAMINATION RESULT FORM

We have read the thesis entitled **"SEAWATER EFFECT ON BEHAVIORS OF IMPACT AND AXIAL COMPRESSION-AFTER IMPACT OF COMPOSITE PIPES"** completed by **MEHMET EMİN DENİZ** under supervision of **PROF. DR. RAMAZAN KARAKUZU** and we certify that in our opinion it is fully adequate, in scope and in quality, as a thesis for the degree of Doctor of Philosophy.

Prof. Dr. Ramazan KARAKUZU

Supervisor

Prof. Dr. Onur SAYMAN

Thesis Committee Member

Assoc. Prof. Dr. Mustafa TOPARLI

Thesis Committee Member

Prof. Dr. Muzaffer TOPÇU

Examining Committee Member

Assoc. Prof. Dr. Bülent Murat İÇTEN

Examining Committee Member

Prof. Dr. Mustafa SABUNCU
Director
Graduate School of Natural and Applied Sciences

ACKNOWLEDGMENTS

I would like to thank my academic advisor, Prof. Dr. Ramazan Karakuzu, for his continuous encouragement, valuable advice and support throughout the course of this study from whom I learned so much. I would also like to thank Prof. Dr. Onur Sayman and Assoc. Prof. Dr. Mustafa Toparlı for the useful discussions on periodical meetings of this study.

I want to acknowledge Assoc. Prof. Dr. Bülent Murat İçten, Assoc. Prof. Dr. Cesim Ataş, Dr. Yusuf Arman and Assist. Prof. Dr. Mehmet Aktaş their valuable advises, and I have received tremendous assistance from Research Assistant Mustafa Özen during the tests. I want to express my gratitude to those who has worked in the Mechanic program at Department of Mechanical Engineering in Dokuz Eylül University.

I thank to Chief Inspector of the Department of Labor Occupational Safety and Mechanical Engineer Metin Avcıoğlu (M.Sc) for the supply of barrels.

The work described in this thesis is financially supported by The Scientific and Technological Research Council of Turkey (TÜBİTAK), (Project Number: 108M471).

Most of all, I thank my parents and parents-in-law for all of the encouragement and support they have provided.

I would like to gratefully acknowledge this support. Finally very special thanks to my wife and my children, who continuously have been very supportive and patient during the period of my study.

Mehmet Emin Deniz

SEAWATER EFFECT ON BEHAVIORS OF IMPACT AND AXIAL COMPRESSION-AFTER IMPACT OF COMPOSITE PIPES

ABSTRACT

The aim of this thesis study is to investigate the effect of the seawater on impact behavior and axial compression after impact strength of the composite pipes having four different diameters and approximately 1.75 mm wall thickness. E-Glass/epoxy pipes with $[\pm 55^{o}]_3$ orientation were fabricated using filament winding process.

Specimens, dry and immersed in seawater for 3-, 6-, 9-, and 12-month, were subjected to transverse impact having 15J, 20J, and 25J energies, using instrumented Fractovis Plus impact testing machine at the room temperature. Following, variation of contact force versus time, contact force versus deflection, contact force versus seawater immersion time, absorbed energy versus seawater immersion time, maximum deflection versus seawater immersion time, and contact time versus seawater immersion time for above impact energies are driven.

Also, the axial compression after impact tests was carried out by using Universal Shimazdu AG-X testing machine and the compressive strength versus seawater immersion time diagrams is driven. Results show that the seawater has significant effects on transverse impact behavior and the compressive strength of the composite pipes.

Keywords: Composite pipe, Filament winding, Transverse impact, Seawater effect, Compressive strength

KOMPOZİT BORULARIN DARBE VE DARBE SONRASI EKSENEL BASI DAVRANIŞINA DENİZ SUYU ETKİSİ

ÖZ

Bu tez çalışmasının amacı, dört farklı çap ve yaklaşık 1,75 mm et kalınlığına sahip kompozit borularda deniz suyunun darbe davranışına ve darbe sonrası bası mukavemetine etkisini incelemektir. Cam/epoksi borular, $[\pm 55^{o}]_3$ fiber oryantasyonuna sahip olup filament sarma işlemiyle üretilmiştir.

Deney numuneleri kuru, 3, 6, 9 ve 12 ay deniz suyunda bekletildikten sonra Fractovis Plus darbe test cihazı kullanılarak oda sıcaklığında 15J, 20J ve 25J darbe enerjilerinde darbe testlerine maruz bırakılmıştır. Darbe testlerinin akabinde, temas kuvveti-zaman, temas kuvveti-çökme, temas kuvveti-deniz suyunda bekletilme süresi, absorbe edilen enerji-deniz suyunda bekletilme süresi, maksimum çökme-deniz suyunda bekletilme süresi ve temas süresi-deniz suyunda bekletilme süresi üç farklı darbe enerjisi için oluşturulmuştur.

Bunun yanı sıra darbe öncesi ve darbe sonrası eksenel bası testleri Universal Shimazdu AG-X test cihazı kullanılarak gerçekleştirilmiştir. Testlerden sonra bası mukavemeti-deniz suyunda bekletilme süresi grafikleri elde edilmiştir. Sonuç olarak kompozit boruların darbe davranışı ve bası mukavemeti üzerine deniz suyunun önemli etkiye sahip olduğu görülmüştür.

Anahtar sözcükler: Kompozit boru, Filament sarma, Enine darbe, Deniz suyu etkisi, Bası mukavemeti

CONTENTS

Page

CHAPTER ONE
INTRODUCTION

1.1 Overview

Filament wound fiber reinforced composite materials increasingly find many application areas such as pressure vessels, pipe lines, rocket motor casing, wind turbine towers etc., because of their extremely high strength to weight ratio. However, these structures are susceptible to some loadings such as compression, impact loading or compression after impact loading along in-plane direction either during handling or in-service.

Despite the fact that most composite structures are rarely completely flat in practice, most of the research has been focused on plate and beam structures; while relatively little research has been carried out on composite shell structures, so far. Also post impact behaviors, environmental (seawater) effects and compressive strength behaviors of composite pipes are little studied.

In this context, the literature review covers relevant previous and ongoing work done by different researchers on the impact characteristics, compressive strength of glass fiber reinforced plastic (GFRP) pipes. Literature review regarding the effect of seawater on the mechanical properties, impact response and compressive strength behavior of GFRP is presented.

(Zhang & Mason, 1999) investigated the effects of pollutant on the mechanical properties of the carbon fiber reinforced structural composites. As a pollutant, water, seawater, acid, alkaline and organic solvent were used and samples were exposed to this pollutant both before and after curing. Decreasing the mechanical properties by the effects of pollutants was obviously seen. Wu et al. (2002) studied on mechanical performance of the glass/vinylester composites which exposed to without ion water, seawater, and synthetic seawater. They were observed that there were the highest decrease in interlaminar shear strength and tensile strength because of the effect of

without ion water and seawater, respectively. (Kootsookos & Mouritz, 2004) investigated the seawater influences on durability of the carbon fiber reinforced composites, experimentally. They were used composite materials as glass/polyester, carbon/polyester, glass/vinylester and carbon/vinylester. They had seen chemical degradations in the resin matrix and the fiber/matrix interface. As a result of these, the bending modulus and strength of the composite were reduced. (Soutis & Turkmen, 1997) evaluated the compressive response of the T800/924C carbon fiber/epoxy composite in the hot-wet environment. They had observed that failures of specimens tested occur because of out-of-plane fiber micro buckling. Also, they observed a decreasing of the matrix strength in the high temperature. The effects of water absorption on properties of glass fiber reinforced plastic (GRP) pipes were investigated by (Yao & Ziegmann, 2007).

(Strait, Karasek, & Amateau, 1992) studied the effect of seawater immersion on the impact response for two glass fiber reinforced epoxy composites which consist of continuous non-woven E-glass/epoxy and woven E-glass/epoxy. They were obtained that moisture-induced degradation was significantly reduced the impact response for both E-glass/epoxy composites. The effect of water absorption on impact behavior of two different woven glass-aramid-fiber/epoxy composites was investigated by (Imielinska & Guillaumat, 2004). They were aimed to assessment impact damage tolerance, depending on the type of glass-aramid reinforcement and laminate conditioning. It is seen that impact damage area was slightly less extensive in wet specimens, which is suggested to be the result of the propagation of interfacial damage present in wet specimens prior to impact, which absorbed impact energy and inhibited the delamination formation. The least sensitive specimen to impact damage was wet specimens of interlaminated composites. It is seen that experimental results of residual compression strengths compare well with predictions based on a simple empirical model. (Deniz, Karakuzu, Sari, & Icten, 2010) studied on the effects of the seawater and transverse impact on axial compressive strength of the composite pipes having 100 mm inner diameter. Glass/epoxy pipes with $[\pm 55^{o}]_3$ orientation were fabricated using filament winding process. Specimens dry and immersed in seawater for 3 and 6 months were subjected to impact having 15J, 20J, and 25J impact

energies. The axial compression impact tests were carried out. They obtained that the seawater and transverse impact have significant effect on the compressive strength of the composite pipes. (Deniz, Karakuzu, Sari, & Icten, 2011) were carried out the effects of the tube diameter and the impact energy level on the impact and axial compressive strength of glass/epoxy composite tubes, experimentally. It is seen that both specimen diameter and impact energy highly affects impact response and compressive strength of composite tubes. Gning et al. (2005) performed quasi-static and impact indentation tests on thick [±55] filament wound glass/epoxy tubes for underwater applications, experimentally. Tubes used in the tests had a 55 mm internal diameter, 6 mm wall thickness and the impact energies up to 45 J. They obtained damage because of the implosion pressure and a critical impact energy level in implosion resistance.

Impact response of laminated composite cylindrical shells was determined by (Krishnamurthy, Mahajan, & Mittal, 2003) using a classical Fourier series and the finite element methods. (Zhao & Cho, 2004) investigated the impact-induced damage initiation and propagation in the laminated composite shells for low-velocity impact. The damage analysis was performed by using the Tsai-Wu quadratic failure criterion. In their study, flat and curved laminates compared for discussing on damage mechanism. Obtained results are shown that numerical results were validated with experimental results. Static response characteristics and impact response of thin fiber reinforced composite cylindrical panels were investigated by (Kistler & Waas, 1999) using linear and nonlinear plate theory. It was seen that the static response was a lower limit to the impact response and can give insight into low velocity impact response behavior. (Kistler & Waas, 1998) studied on the response of curved laminated composite panels subjected to low velocity impact, experimentally and mathematically. Therefore, they examined both small and large deformation. A nonlinear system of equations was derived for the impact problem and impact tests were also performed to validate the analyses. So, impact force and displacement histories were compared with the test data and the studies of other researchers for small and large deformation of flat and curved panels. (Khalili, Soroush, Davar, & Rahmani, 2011) investigated laminated composite plates and cylindrical shells

subjected to low-velocity impact by numerical analysis using ABAQUS finite element code.

(Tarfaoui, Gning, & Collombet, 2007) presented a finite element code of static and dynamic tests on thick filament wound glass/epoxy tubes. They used certain models for validating material characteristics to predict their elastic behavior for static and dynamic loadings and further, they developed an impact model including material property degradation for progressive damage. (Gning, Tarfaoui, Collombet, & Davies, 2005) have firstly identified damage initiation and damage progression in the glass-epoxy composite cylinders subjected to drop weight tests. After that, they have conducted compression after impact tests by hydrostatic pressure and damage was evaluated. Chib (2003), investigated the low velocity impact simulation on carbon/epoxy composite tubes with nonlinear explicit finite element code, LS-Dyna. Also, experimental results were validated with the finite element model. As a result, study demonstrated the accuracy and effectiveness of impact test on tubes with LS-Dyna and good predicting with obtained results for various parameters as impactor velocity, lay-up configuration and boundary conditions.

(Doyum & Altay, 1997, 1998) investigated the detection possibility of different types of defects produced as a result of low-velocity transverse impact loading on $(\pm 45^{o}_{2}, 90^{o})$ S-glass and $(\pm 54^{o}_{3}, 90^{o})$ E-glass fiber-reinforced epoxy tubular composites. Visual inspection, water-washable red dye, water-washable fluorescent and post-emulsified fluorescent penetrant systems were utilized for damage detection. Cracks of different sizes and delamination zones caused by impact were detected using the above-mentioned non-destructive inspection techniques. The dynamic behavior and impact damage of laminated composite shells with various curvatures and stacking sequences were investigated by (Kim, Goo, & Kim 1997). A three-dimensional finite element code was developed to describe the dynamic and impact response of shell-shaped structures. The results were compared with those of plates of the same dimensions and stacking sequences. As the curvature increases, the maximum impact force becomes higher for the same impact velocity. Although the delamination patterns of the cylindrical shell have a similar tendency to those of

the plates, the delaminated area widens as the curvature increases. Schultz (1998), studied energy absorption capacity of graphite-epoxy composite tubes with circular and square cross-sectional geometries having stacking sequences with ±45° fibers and with both ±45° and 0° fibers subjected to both static and dynamic crushes to examine the energy absorption characteristics. The geometry had a significant effect on the energy absorption. (Gong, Lam, & Reddy, 1999) studied impact response of cylindrical shells using an analytic solution. The solution includes contact and transverse shear deformation.

(Palmer, Neilson, & Sivadasan, 2006) described two experimental programs as development of a semi-empirical and dimensionally consistent perforation correlation. Therefore, two programs can be compared with British Gas tests on a much longer pipe. Palmer et al. (2006) studied that a pipeline under construction might accidentally fall on an existing pipeline operation. So, they carried out to study what would happen, and to reassure the operator that the existing line would not be ruptured. (Changliang, Mingfa, Wei, & Haoran, 2006) investigated the impact behavior of the composite filament cylindrical vessel with metal liner with and without internal pressure using a 3D nonlinear finite element method. Results showed that low-velocity impact damage had more effect on vessel with the internal pressure conditions. (Zeng, Fang, & Lu, 2005) carried out the impact energy absorption of 3D braided composite tubes subjected to axial impact and simulation of collision behavior using a LS-DYNA program. They investigated effects of the geometric and braid parameters on energy absorption characteristics. The obtained results were compared with the experimental data and a good agreement was observed. Effect of seawater on compressive strength of concrete cylinders reinforced by non-adhesive wound hybrid polymer composites (Liu, Tai, & Lee, 2002). Both material type and environmental condition could influence the strength reduction of composite/concrete system subjected to seawater absorption or air aging. They were seen that there is no obvious difference for the effect of live or dead seawater soakage on strength reduction of specimens.

(Tarfaoui, Gning, & Hamitouche, 2007); (Tarfaoui, Gning, Davies, & Collombet, 2008) examined static and dynamic analysis of the thick filament woud glass/epoxy tubular structures, experimentally and numerically using ABAQUS. Scale and size effects on dynamic response and damage were investigated. Simulated damage was compared with that of obtained experimentally. It is seen that the numerical and experimental results were found to be in good agreement. The buckling of cylindrical shells with through cracks was studied by (Estekanchi & Vafai, 1999). They developed a special program for generating finite element models of cylindrical shells according to crack length and fiber orientation. The results of the analysis were presented in parametric form when it seems to be appropriate. Sensitivity of the buckling load to the crack length and orientation has also been investigated. (Matemilola & Stronge, 1996) studied impact response of a simply supported composite cylinder with by analytical solution. Numerical examples for both thick and thin cylinders showed that local contact deformation was important for an accurate solution of the impact response. The compressive properties and crushing response of square carbon fiber reinforced composite tubes subjected to axial compression and impact loads have been investigated by Mamalis et al. (2006) using the LS-DYNA3D explicit finite element code. Xu et al. (2009) studied the local and global buckling of cylindrical shells under axial, compressive impact loads. It was found that critical buckling loads were affected by radial inertia, which tends to increase the critical loads. (Huang & Wang, 2009) conducted quasi-static tests on carbon reinforced composite tubes first to examine their axial crushing response, experimentally. Then numerical simulations were performed and compared with experimental data to investigate how to establish an effective model for predicting energy absorption behavior and crushing failure mode of the tubular composites. Khalid (2001), investigated axial crushing behavior of hybrid composite tubes, experimentally and numerically. A comparison was done for between the finite element and the experimental results. As a result, it is seen that carbon fiber reinforced tubes stands to higher loads than glass fiber and cotton fibers. On hybrid type tests, tubes with the external layer of carbon have shown higher strength than those of internal carbon fiber layers. Experimental quasi-static crushing and finite element analysis had been carried out by Mahdi et al. (2003). Cotton/epoxy tubes

with different diameters (50, 70, 90, 110, and 130 mm) and fiber orientation angles (80° and 90°) were used. Results indicate that the tube with fiber orientation of 80° and outer diameter of 130 mm shows the best load-carrying capacity at initial crush stage and the amount of energy absorbed by the tube depends on the crushing mechanism.

1.2 Objectives of the Present Research

The primary objective of this work is to investigate the effects of the seawater and transverse impact on the axial compressive strength of $[\pm 55°]_3$ filament-wound glass/epoxy pipes, experimentally. Specific objectives of the dissertation research are also as follows:

1. To find gain of seawater by pipes immersed seawater for four different environmental times.
2. To obtain the effect of impact energy on the compressive strength after impact of glass/epoxy composite pipes.
3. To obtain the effect of specimen diameters on impact behavior of composite pipes.
4. To investigate the effect of seawater on impact behavior of composite pipes.
5. To obtain the effect of specimen diameters on axial compressive strength after impact.

1.3 Sponsorship

This thesis is sponsored by The Scientific and Technological Research Council of Turkey (TÜBİTAK), (Project Number: 108M471).

CHAPTER TWO
IMPACT ON COMPOSITES

2.1 Introduction

Composite materials consist of two or more materials which together produce desirable properties that can not be achieved with any of the constituents alone. Composites are commonly classified based on the type of matrix used: polymer, metallic and ceramic. In fiber-reinforced composite materials, for example, consist of high strength and high modulus *fiber* in a *matrix* material. In these composites, fibers are the principal load carrying members, and the matrix material keeps the fibers together, acts as a load-transfer medium between fibers, and protects fibers from being exposed to the environment (e.g., moisture, humidity and corrosion etc.) (Reddy, 1997).

During the life of a structure, impacts by foreign objects can be expected to occur during manufacturing, service, and maintenance operations. So, impacts create internal damage that often can not be detected by visual inspection. This internal damage can cause severe reductions in strength and can grow under load. Therefore, the effects of foreign object impacts on composite structures must be understood, and proper measures should be taken in the design process to account for these expected events (Abrate, 1991).

2.2 Composite Pipes

Composite pipes made of fiber reinforced plastics have many potential advantages over pipes made from conventional materials. The use of fiber reinforced composites in various applications has been in practice in recent years. The use of these pipes for underwater applications (underwater vehicles, oceanography, subsea installations for the transportation of seawater, oil, natural gas and other process fluids, etc.) is very attractive, for the light weight, high specific stiffness and strength, good corrosion resistance and thermal insulation. Engineers may be faced with the ongoing task of

rehabilitation pipelines due to damage caused by many environmental and various loads as transient impact, either during handling or in-service.

2.3 Filament Winding Process

Most composite pipes are manufactured by filament winding process. Filament winding process consists of winding continuous-fiber roving or roving tape over a rotating male mandrel at the desired angle. The mandrel rotates at a speed necessary to generate. The fibers are first fed through a resin bath or pre-impregnated with partially cured resin and then continuously wound onto a mandrel under controlled tension.

The types of filament winding process used for circular cross-section products are follows:

- Wet winding,
- Dry winding,
- Wet re-rolled winding

There are also a number of different winding methods or patterns, primarily helical winding, polar winding and hoop or circumferential winding (Mantel & Cohen, 2000).

The most common products manufactured by the filament winding process are pressure vessels, rocket motor cases, engine cowlings, tubular structures, pipes, and chemical storage tanks etc.

2.4 Material

2.4.1 Fiber

The most common reinforcement for the polymer matrix composites is glass fibers. The glass fibers are divided into three classes as E-glass, S-glass and C-glass.

- E-glass (electrical) has a good strength and stiffness, the lowest cost fiber, good electrical properties and is available in many forms, but impact resistance is relatively poor. E-glass reinforcing fiber is mostly used in filament winding (pipe manufacture).

- S-glass (tensile strength) has better strength and modulus than E-glass, higher cost fiber, and commonly used in aerospace, defense industries, and high performance pressure vessel applications.

- C-glass (chemical) has the best resistance to chemical attack and high corrosion resistance, is mainly used in the form of surface tissue in the outer layer of laminates and used in chemical and water pipes and tanks.

In this study, E-glass fiber was used as reinforcing of the composite pipes.

2.4.2 Resin (Matrix)

Nowadays, typical matrix materials constituents from polymeric, metal, carbon and ceramic materials, polymeric matrices are divided into two main types, thermoset and thermoplastic. Thermoset polymers consist of three types use in the composite manufacture, namely polyester, vinylester and epoxy.

- Epoxy is a thermoset that cures when mixed with a catalyzing agent or hardener. It is known for their excellent adhesion, many type’s available, good chemical and heat resistance, higher material cost, good to excellent mechanical properties and very good electrical insulating properties.

- Polyester is low-cost resin systems and it has good corrosion resistance, good strength.

- Vinylester is widely used for composite manufacture. It is a chemical combination of epoxy and polyester technology. They offer good chemical and corrosion resistance, superior strength and toughness properties. But, it is higher cost.

In this investigate, epoxy resin were selected for using in manufacture of composite pipes.

2.5 Effect of Seawater on Composite Pipes

Seawater degradation may cause swelling and plasticization of the epoxy matrix and debonding at the fiber/matrix interface that may reduce the mechanical properties. Moisture absorption amounts depend on the concentration of salt; the higher salt concentration can produce a lower change in moisture absorption amount. Composites are usually used in marine applications such as oil and natural gas transportation, naval mine hunting ship. Seawater absorption is an important parameter in the degradation of polymeric composites applied in marine field.

The gain of the seawater content enhances the probability of material degradation which generally follows three main mechanisms:

- Direct diffusion of water molecules through the matrix and, in some cases, through the fibers.
- Capillary flow of water molecules along the fiber/matrix interface followed by diffusion from the interface into the bulk resin. This is a consequence of debonding mechanisms between the fibers and matrix caused by water attack at the interface.
- Diffusion through micro cracks, pores, defects in the material (Zhou & Lucas, 1995).

In the material response to the overall moisture absorption process, cracks (including surface voids) and the surface mass loss (including surface peeling and dissolution) has great influence on the apparent weight change behavior. Surface peeling and resin dissolution contribute to weight loss (a net decrease of the overall weight) of the specimen, whereas surface crack and voids between fibers trap water thus promoting weight increase.

2.6 Behavior of Composites under Impact Load

Composites consist of two sub materials as fiber and matrix. Fiber and matrix properties significantly affect the damage initiation and propagation due to affect the overall and contact stiffness of the composite structure. In addition to properties of the materials, a lot of parameters are considered in the literature. The thickness, size, and the stacking sequence of the laminate, the density, elastic properties, shape and initial velocity of the impactor, and also stitching, environmental conditions such as temperature and humidity are all factors that influence the damage characteristic of the composite materials (Abrate, 1998).

Fiber-reinforced composites are very sensitive to transverse loading because they are much weaker in the thickness direction than in the lamination. Consequently, composites subjected to transverse impact may suffer significant in plane damage, resulting in deterioration of its overall load-carrying capacity. The response of composites to these impact loadings is complex, as it depends on the structural configuration as well as the intrinsic material properties. Further, it depends on the material, geometry, and velocity of the impactor. Each one plays an important role in characterizing the overall effect of transverse impact.

It is known that behavior of composites under impact loading has been studied especially during last two decade by many researchers. Some review articles and books on the subject covering impact response, contact laws, impact dynamics, damage mechanics, structural dynamics, damage initiation and propagation, stability,

failure modes, damage tolerance, and micromechanics can be found in literature (Abrate, 1991, 1994, 1998; Cantwell & Morton, 1991).

During impact event, the various forms of damage modes (such as matrix cracking delamination and/or fiber breaking) are possible under impact loading range from invisible or barely visible to penetration of the impactor. So, at the moment in use, two types of tests are used by most investigators, although many details of the actual test apparatus many differ. Experimental studies attempt to replicate actual situations under controlled conditions. For example, during aircraft take-off and landing, debris flying from the runway can cause damage; this situation, with small high-velocity projectiles, is best simulated using a gas gun. Another concern is the impact of composite structure by a larger projectile at low velocity, which occurs when tools are accidentally dropped on a structure (Abrate, 1998). For low velocity impacts may not cause significant damage on the composite during the early stage of the impact. But, these may cause internal damage in the form of matrix cracking, delamination, and/or fiber cracking inside of the composite. These damages may lead to significant reduction in strength and stiffness of composite.

Low velocity impact normally produces structure deformation during the contact duration of the impactor, and this situation is considered quasi-static with no consideration of the stress waves that propagate between the impactor and the boundary of the impacted component (Naik, 2005). Impact test can be conveniently divided into three main categories as low velocity, high velocity and hyper velocity impact. However, there is no clear definition to determine the limits of these categories. Sjoblom et al. (1988), Shivakumar et al. (1985), and (Cantwell & Morton, 1991) have defined the low velocity impact as up to 10 m/sec. However, Abrate (1991) in his review article determined the low velocity impact as the impactor speed is less than 100 m/sec. (Liu & Malvem, 1987) and (Joshi & Sun, 1987) have suggested that type of impact can be classified according to the damage occurrence. Low velocity is characterized by delamination and matrix cracking while high velocity is by penetration induced fiber breakage. Currently, however, increasing use is being made of instrumented impact tests with drop weight impact testers to characterize the low velocity impact of composite structures. This is usually done on

drop weight impact machines, where the striker is instrumented to measure the applied load. These machines have means of measuring displacement or acceleration. Thus the history of the load, displacement, and acceleration during the impact event is recorded, and these can be converted to give impact load-time and impact energy-time histories. From these, features such as peak load and absorbed energy can be related to fracture processes occurring in the material (Naik, 2005).

When the impact event leads to complete pulverization of the projectile and target materials, in the immediate vicinity of the contact, then the impact event is named as hyper velocity impact. Generally, hyper velocity impacts are said to occur for impactor speeds larger than 1 km/sec (Abrate, 1991).

Recent studies show that penetration or perforation can be caused in the velocities were less than 5 m/sec in experiments. Because of the confusion in determination of impact, the first definition by (Cantwell & Morton, 1991), mentioned above is selected. It means all of the experiments in their study were assumed as low velocity impact. The main objective of the study is to improve the energy absorption capacity of laminated composite plate not determination of limits of impact event.

2.7 Failure Modes

During impact tests, the damage modes can be classified two parts as macroscopic and microscopic viewpoints. Macroscopic damage modes are described as indentation, penetration, perforation, and bending fracture. *Indentation* is damages with interlayer and intralayer matrix cracks in the impacted point. *Penetration* is sticking and *Perforation* is making a hole into specimen by impactor nose. For the penetration case, specimen absorbs all of the impact energy and at the maximum deflection of the midpoint of the specimen the velocity reaches zero. But, at the perforation case, the impactor moves after impact event due to the all of the impact energy not absorbed by specimen. Namely, in the penetration and perforation cases, there is no elastic energy returning to the impactor. *Bending fracture* has damage shape more like a line. In microscopic viewpoint, impact damage consists mainly of

matrix-controlled, failure modes can be specified as matrix failure, delamination and fiber breakage. These damage modes may lead to significant reduction in strength and stiffness (Icten, 2006; Aktas, 2007).

A typical load versus time curve obtained by an instrumented impact test is schematically shown in Figure 2.1. The load-time curve can be conveniently divided into two regions. First and other regions represent of fracture initiation phase and fracture propagation phase, respectively.

Fracture initiation at or near the peak load occurs either by the tensile failure of the outermost fibers or by interlaminar shear failure. These failure mechanisms on a microscale for example, microbuckling of the fibers on the compression side of the specimen or debonding at the fiber-matrix interface are possible. When critical load reached peak force, initiation fracture phase represents propagation fracture phase. At this phase the composite specimen may fail either by a tensile failure or a shear failure due to the relative values of the tensile and interlaminar shear strengths. At fracture propagate phase either in a catastrophic “brittle” manner or in a progressive manner continuing to absorb energy-at smaller loads (Naik, 2005; Mallick, 1993; Mahdi et al., 2003).

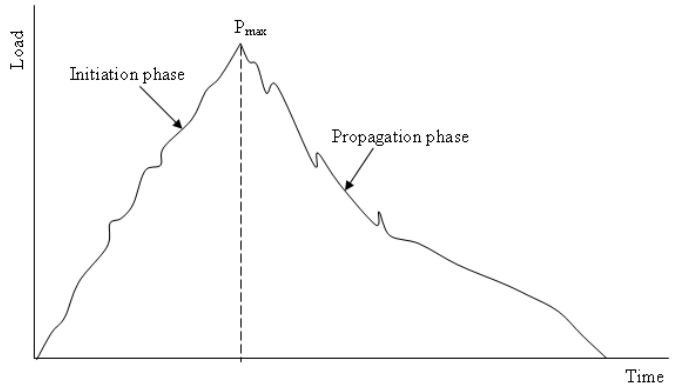

Figure 2.1 Typical load-time curve obtained an instrumented impact test

In the impact load, the epoxy is a more breakable sub material than the fibers in composites. Therefore, after impact, the damage process initiates matrix cracks which then induce delaminations at ply interfaces. In impact event, two types of matrix cracks were observed as tensile cracks and shear cracks (Figure 2.2). Tensile cracks are introduced when in-plane normal stresses exceed the transverse tensile strength of the ply. Shear cracks are at an angle from the mid-surface, which indicates that transverse shear stresses play a significant role in their formation.

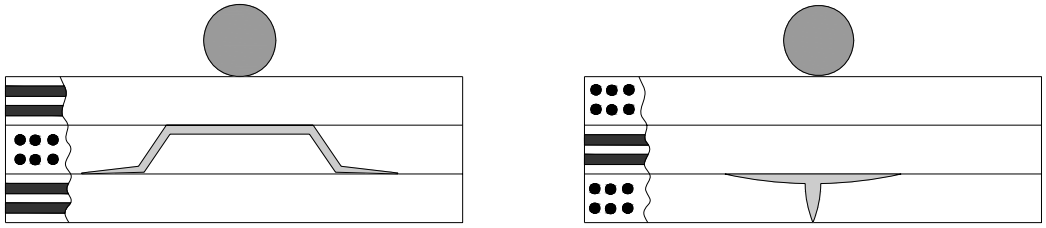

(a) **(b)**

Figure 2.2 Two types of matrix cracking; **(a)** shear crack, **(b)** tensile crack (Abrate, 1998)

In thick laminates, matrix cracks occur in the first layer impacted by the impactor because of the high and localized contact stresses. Therefore, damage progresses like a pine tree pattern from the top to down (Figure 2.3-a). Besides, in thin laminates, matrix cracks can be introduced in the lowest layer due to the bending stresses in the back side of the laminate (Figure 2.3-b). So, damage again starts a pattern of matrix cracks and delaminations and leads to a reversed pine three pattern (Abrate, 1998).

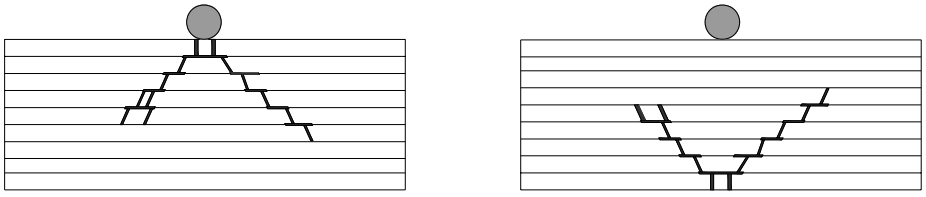

(a) **(b)**

Figure 2.3 Pine tree and reversed pine tree patterns **(a)** for thick laminate **(b)** for thin laminate (Abrate, 1998)

Delamination is the debonding between adjacent laminas. Delaminations may occur at interfaces between plies with different fiber orientations and delamination initiates at the intersection of a matrix crack with the ply interface. This way, when

two adjacent plies the same fiber orientations, delamination will not introduce at the interface between plies. Strength of the laminate reduces due to this damage (Abrate, 1998).

A typical characteristic of a delamination is given in Figure 2.4. The delamination type appears as a peanut. The delamination elongation is oriented in a fiber direction. In impact event, delamination damage usually occurs at the back face of the laminate and progressively becomes smaller toward the impact face.

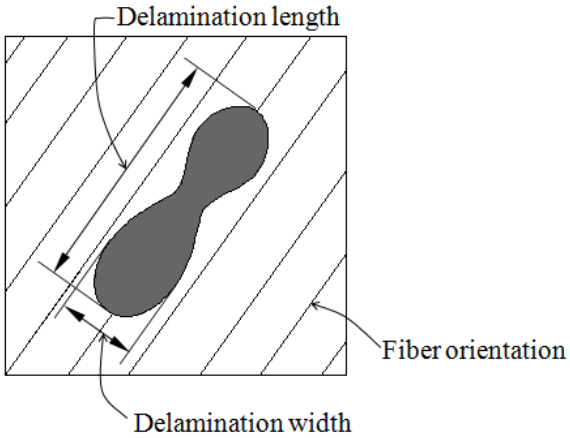

Figure 2.4 Typical delamination shapes

2.8 Failure Modes under Axial Compression Load of Composites

Axial compression after impact test is an experimental prediction of the degradation of the compressive strength of the composite pipe due to axial loading. In this load case, compressive strength reduction is the largest. So, axial compression loading is considered to be one of the most important topics in the design of composite pipes. Compressive strength is very important property for especially delaminated specimen. Delamination decreases the compressive strength of the layered composite.

The compressive strength of the composites decreases with increasing immersion time. It may be explained with seawater absorption and chemical degradation of resin

matrix and fiber-matrix interphase region (Kootsookos & Mouritz, 2004). One more time the damage induced by impact load is more affect on compressive strength than the water immersion effect (Deniz et al., 2010). The pipe with the largest diameter was observed to fail purely due to local buckling mode. But, when the specimen diameter decreases, the failure mode gradually changes to global buckling mode and mixed buckling failure modes may be caused as well.

CHAPTER THREE
EXPERIMENTAL METHODS

3.1 Introduction

This chapter deals with the experimental overview of the thesis. Experimental study will be presented in four subchapters. The first chapter is about the production method and preparation of the composite specimens. The second chapter is about the impact characterization of the composite specimen. The third chapter is about the compressive strengths before/after impact of the composite specimens. Specimens are exposed to environmental condition (seawater), which is mentioned in the last subchapter.

3.2 Manufacturing of Composite Pipes and Specimen Preparation

Glass fiber reinforced composite pipes with $(\pm 55^{o})_3$ winding angles and band width of 11 mm were manufactured using a CNC filament winding machine in Izoreel Firm. A filament-winding machine was used to conduct glass roving onto the mandrel through a tension controller with fiber tension. The fiber roving was impregnated by epoxy resin before winding onto a metal cylindrical mandrel (Figure 3.1). A continuous roving of E-glass-fibers with the fiber diameter of 17 μm and 600 Tex were adopted for the filament winding process. Epoxy EPR 828 EL resin and EPH 875 hardener was selected as matrix. The mechanical properties of the fiber and matrix materials are listed in Table 1. The curing was carried out by using an oven at 130^{o}C for 3 h on a mandrel in a slow motion rotary oven. Then, the pipe was cooled to room temperature with the same rotary velocity and after then pulling out the mandrel. The fiber volume fraction (V_f) and density of the pipes studied in this investigation were about 65% and 2.08 g/cm^3, respectively.

Table 3.1 Mechanical properties of the fiber and resin

	E (GPa)	σ_{TS} (MPa)	ρ (g/cm^3)	ε_t (%)
E-glass	73.0	2400	2.6	4-5
Epoxy resin	3.4	50-60	1.1	6

Figure 3.1 CNC filament winding machine and composite pipe

Specimen was cut out from a 1 m length composite pipe to obtain specified test length using a diamond wheel saw. The length of the specimen was 150 mm. The inner diameters of the specimens were selected as 50, 75, 100, and 150 mm. The wall thickness of the specimens was approximately 1.75 mm.

Glass/epoxy composite specimens cut from composite pipes were immersed into seawater. A set of specimens that was not placed in the filled seawater barrels and denoted as ‘dry’ was tested to obtain reference properties. Other specimens were rested on steel barrel and immersed completely in artificial seawater (salinity about

3.5%). The barrel was closed by its cover to prevent the evaporation of seawater (Figure 3.2).

Figure 3.2 Photo of specimens immersed in seawater

3.3 Environmental Conditions

In this study, the effect of immersion in seawater on impact behavior and compressive strength of composite pipe was investigated. Little, if any, information regarding the effects of seawater immersion on the impact resistance and the compressive strength of composite materials has not been published to date.

A set of specimens that was not placed in the filled seawater barrels and denoted as ‘dry’ was tested to obtain reference values. Other specimens were placed in steel barrel and they were exposed to in artificial seawater (salinity about 3.5% at laboratory conditions during 3, 6, 9 and 12 months). After immersion in seawater, the specimens were removed from barrel at different time of period wiped with paper towels to remove the surface water. Then they were weighed. Weight gain was

obtained by measuring the moisture content. Percentage moisture gain was determined as:

$$M\% = \frac{W_e - W_d}{W_d} x100 \quad (3.1)$$

where We and Wd are the weights of specimen exposed to seawater and dry specimen, respectively.

3.4 Impact Test

The Fractovis Plus impact tester was used for low velocity impact tests for this study as shown in the Figure 3.4. The test machine was suitable for a wide variety of applications requiring from low to high impact energies. The impactor, which was used to strike the pipe samples, is a hemispherical indenter with a 12.7 mm diameter is connected to a 22.4 kN piezoelectric force transducer. The total falling mass including impactor nose, force transducer and crosshead was 5.02 kg. The contact force was measured with a force transducer located between the cross head and hemispherical tup nose. An anti-rebounding system is included in the test instrument to stops the impactor after impact to avoid the repeated impact on the specimen. The excessive energy is used to rebound the impactor from the specimen surface at the end of the impact event. The drop-weight test machine has up to 1800J maximum potential energy with the additional mass. Additional energy system can be used to increase the speed of the impactor up to 24 m/s.

(a)

(b)

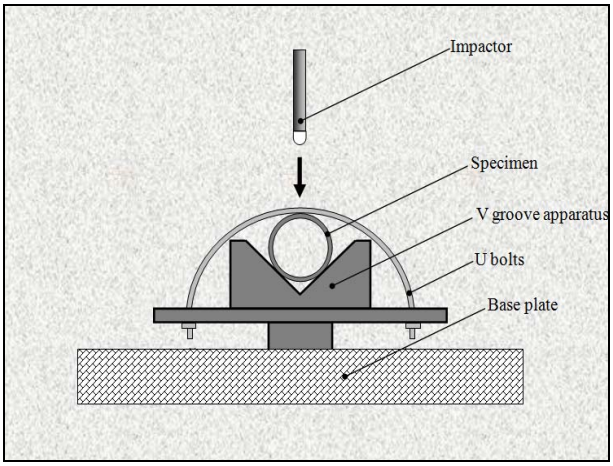

(c)

Figure 3.3 **(a)** Illustration of drop weight impact machine, **(b)** impactor nose (striker) and **(c)** schematic illustration of clamping fixture

In order to carry out the history of the impact event, a data acquisition system (DAS) was utilized. The data acquisition system allows acquiring 16000 data during tests.

The deflection and absorbed energy can be calculated by using a VisualIMPACT software program. The impact force value at each time step, *F(t)*, are recorded by data acquisition system. Deflection derives from a double integration of acceleration as:

$$\delta_i = \iint_i \frac{F(t) - gM_{total}}{M_{total}} dt^2 \qquad (3.2)$$

where δ_i is deflection of the specimen up to point *i, g* is gravity acceleration and M_{total} is total of impact mass.

The relation between the force and the deflection determined by the function, *F(δ)*, which is used for finding the absorbed energy. Namely, absorbed energy *(E_a)* up to point *i* is calculated as the area described under force-deflection curve, *(F-δ)*.

$$E_i = \int_i F(\delta) d\delta \qquad (3.3)$$

Impact failure can be defined by deformation, crack initiation, or complete fracture, depending on the impact test parameters. Failures generally originate at the weakest point in the specimen and propagate from that point. As insufficient energy is delivered to damage the specimen, there is option to either maintain that mass and increase the height or vice versa.

During impact tests, three cases results including *rebounding*, *penetration*, and *perforation* may be carried out (Figure 3.4). At the rebounding case, the contact force reaches the zero and the curve look like a mountain shape. When the impact energy is high enough, perforation will be occurring. At this time, contact force is expected

to be zero. But it does not ever zero due to the friction at the interface of the hemispherical impactor and specimen. At the rebounding case, impact energy is higher than the absorbed energy. So specimen cannot absorb the impact energy that the impactor has. For the penetration case, specimen absorbs all of the impact energy. However, absorbed energy lowers than the impact energy that the impactor has (Icten, 2006).

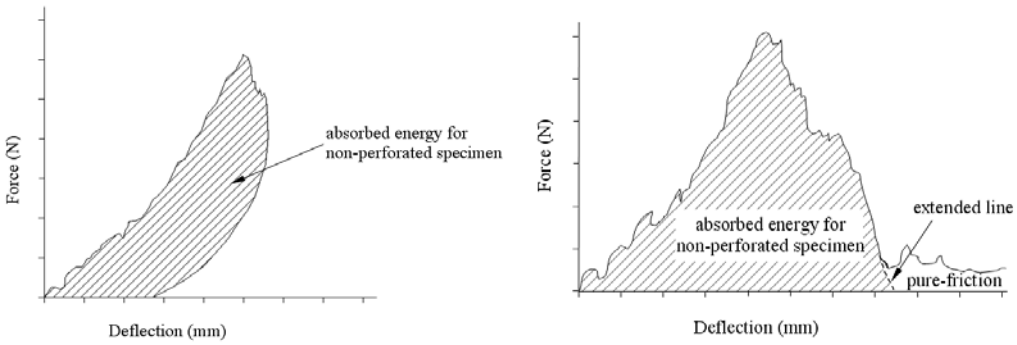

(a) **(b)**

Figure 3.4 Force-deflection curves for calculating the absorbed energy for **(a)** non-perforated specimen, **(b)** perforated specimen (Icten, 2006)

During impact event, maximum (peak) load is the highest point in the force-time history. Often the point of maximum load relates to the onset of material damage or complete failure. Energy to maximum load is the energy that the specimen has absorbed up to the point of maximum load. It is the area under the load/deflection curve from the test start to the maximum load point. Total energy is the energy that the specimen has absorbed up to the end of the test, when the load reaches zero again. It is the area under the load/deflection curve from the test start to the test end. Deflection to maximum load is the distance the impactor traveled from the point of impact to the point of maximum load.

In this study, the impact tests are performed using Fractovis Plus impact test machine in the Composite Research Laboratory of Dokuz Eylül University (Figure 3.3). The impact tests were performed under various impact energies, 15, 20, and 25J, in order to examine damage process in the pipes with various diameters and stacking sequences $[\pm 55^{o}]_3$ at ambient temperature. The impact characteristics such

as force-time, force-deflection curves, and absorbed energy were examined for all the impact energies. The failures of specimens are detected.

Each test was repeated four times and average values were calculated and given in related figures following. Absorbed energy (Ea), maximum contact force, maximum deflection and contact time are four important parameters to evaluate the impact behavior of composite pipes. The time passed during the impact event is named as contact time. Absorbed energy is the energy absorbed by the composite specimen through the impact event by formation of damage inside the specimen.

For the impact test, a special apparatus was developed. The pipe specimen was closed with two glass-epoxy lids to simulate a real long pipe situation and was rest on the groove and fixed to the bottom plate of the apparatus with two U-bolts as shown in Figure 3.7. The description of each individual part used in the experimental facility is discussed in detail in the below.

As shown in Figure 3.5 two difference test fixtures for transverse impact on composite pipes was designed and produced. They have been fabricated using steel. The V-block fixture has a 90° angle. The side supports is of sufficient depth to support the specimen in the V.

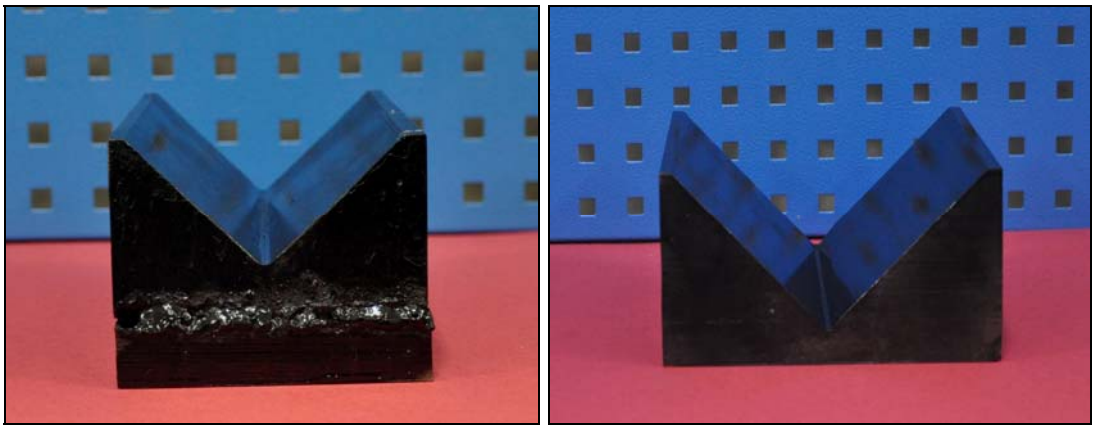

(a) **(b)**

Figure 3.5 V-block test fixtures **(a)** for 50 mm and 75 mm diameters, **(b)** for 100 mm and 150 mm diameters

During impact test, U-bolts were used to prevent moving of the specimen on the V-block fixture. Two U-bolts and nuts are shown in Figure 3.6.

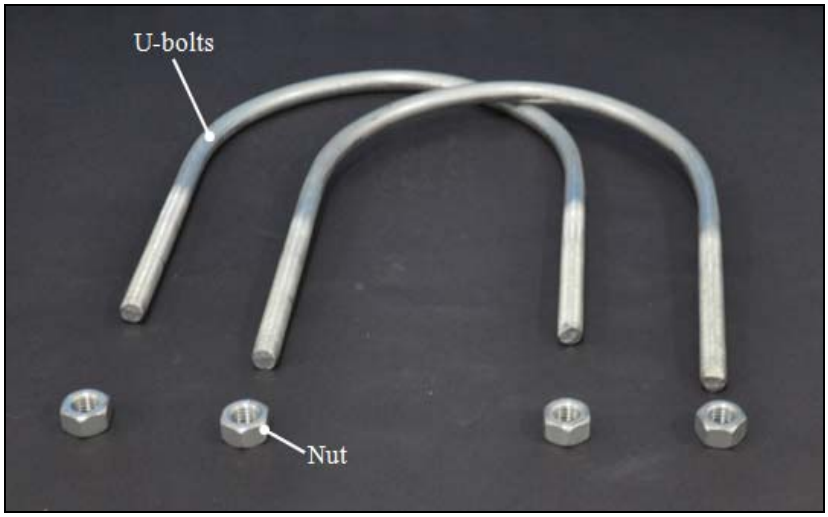

Figure 3.6 U-bolts for impact test apparatus

The ends of the specimen were closed with two glass-epoxy lids to simulate a real long pipe (Figure 3.8). The pipe specimen was placed on the V-groove test fixture with two U-bolts is illustrated as in Figure 3.7.

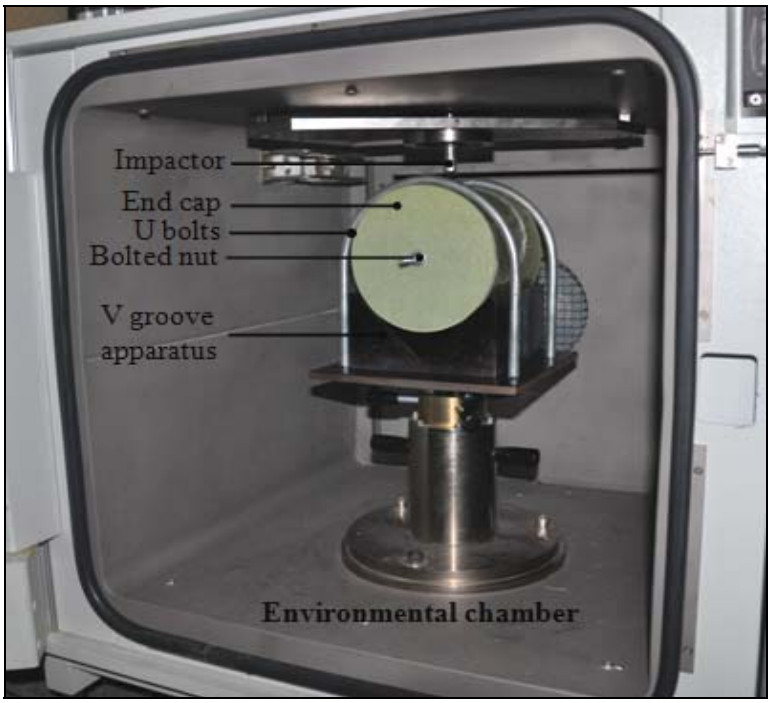

Figure 3.7 V groove test fixture and specimen for impact

(a)

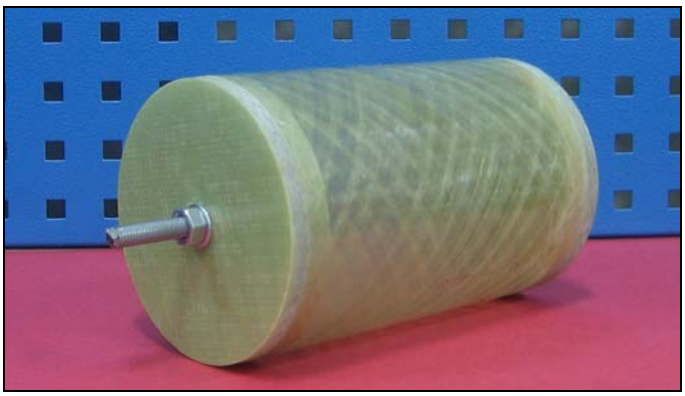

(b)

(c)

Figure 3.8 Illustration of composite pipes and clamp parts **(a)** disassemble of pipe system, **(b)** assemble of pipe system, and **(c)** assemble of the four different diameters specimens

3.5 Axial Compression Test

In this thesis, the axial compression tests are conducted to determine compressive strength of composite specimens. The test was carried out by SHIMADZU tension-compression test machine having capacity of 100 kN in the Composite Research Laboratory of Dokuz Eylül University (Figure 3.11). The load was applied to the specimens at a constant cross-head speed of 2 mm/min. Non-impacted and impacted pipes have been subjected to compression tests until failure. For all cases as impact energy level and environmental condition, each test was repeated four times and average values were calculated.

In the axial compression tests, the applied load measurements were saved on a personal computer which is linked to a machine through a data acquisition system records the force-displacement history. The maximum load is obtained from the force-displacement curve (Figure 3.9). The compressive strength (σ_C) of the specimen is calculated by using;

$$\sigma_C = \frac{F_{\max}}{\pi\left(r_o^2 - r_i^2\right)} \tag{3.3}$$

where $F_{\max}$, r_o and r_i denote the maximum force, the outer diameter and the inner diameter of the test specimen, respectively.

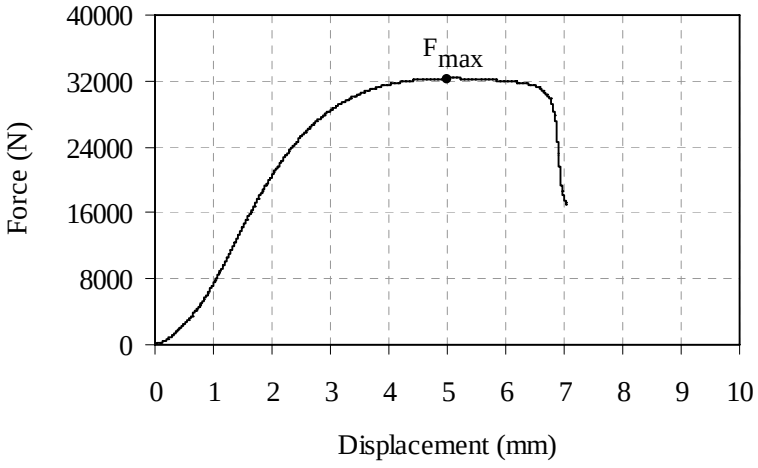

Figure 3.9 Force versus displacement curve for compression test

Suitable damage is expected around the middle surface of the pipe for compression test exists. But, the failure at the end of the pipe that is the contact point between the pipe ends and the plates of the compression test machine. This failure occurs before obtaining the real compression strength of the pipes. To prevent the specimen from this premature failure, the pipes were closed fit with two glass-epoxy end-caps, at the ends as shown in Figure 3.10. Therefore the design of the end-caps was done with utmost care. The end-caps assembly consists of the following parts. The description of each individual part used in the experimental facility is discussed in detail in the below.

The specimen was placed between two rigid steel plates, with compressing materials, which is manufactured from composite, (end caps) between the plate and the specimen. The end cap material was used to avoid premature compressing of the specimen rims. It should be noted that even though the specimen was simply supported, the transverse frictional force between the plates and the cylinder couldn't be avoided. The introduction of the cushioning material further increased the transverse friction. Hence the end conditions simulated in the experiment are considered to be somewhere between the clamped and simply supported end conditions. The test set up used is shown in Figure 3.10 below.

The most critical part in the present compression test is the end cap, because it has to resist a high strength before a last failure occurs in the specimen. For four different diameters, commercial end caps were used as shown in the Figure 3.10, for the first time and the failure of the pipe were found to be at end caps due to weak grip of the end cap gripper. The fibers were damaged under the end caps area due to steel gripper and the pipe became weak on both sides of the pipe and failed. End cap inserted into the pipe specimen.

For different specimen diameters, having 1 mm thickness and 13 mm width the stainless metal clamp with adjustable bolt used are shown in the Figure 3.10, which is mounted in the specimens. The clamps, outside are completely fastened with an adjustable bolt while the end cap assembly is prepared.

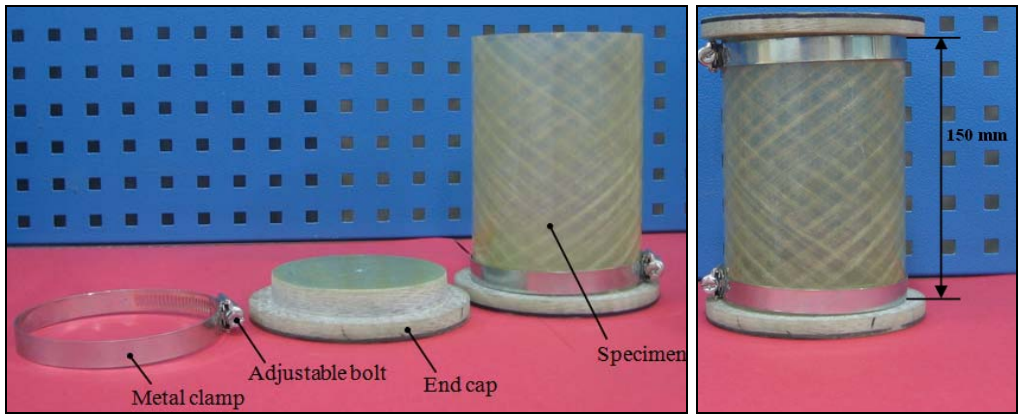

(a) **(b)**

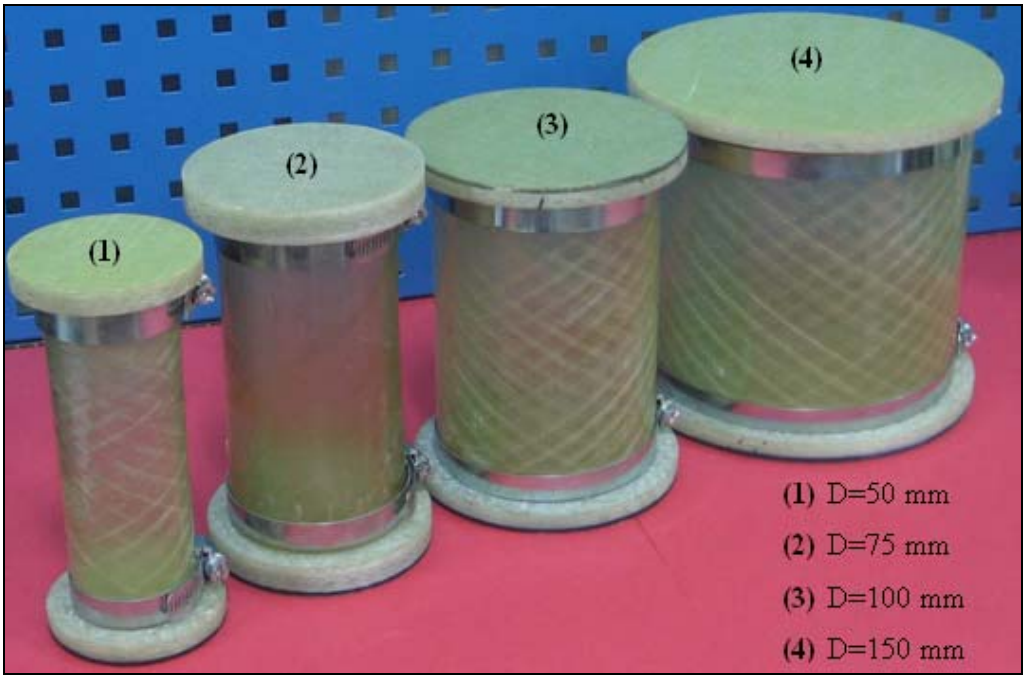

(c)

Figure 3.10 **(a)** Uninstalled clamp parts, **(b)** uninstalled clamp parts, **(c)** view of four different composite pipes and clamp parts

Figure 3.11 Photograph of the Universal tensile-compression test machine

CHAPTER FOUR
RESULTS AND DISCUSSION

4.1 Moisture Absorption

In this study, glass fiber/epoxy composite specimens which were cut from composite pipes a specified length were immersed into seawater for periods of approximately 3-, 6-, 9-, and 12-month. After the end of these time periods the specimens were removed from seawater. Mass change of the samples was recorded using a microbalance accurate to 0.01 mg. The moisture uptake was expressed in percent weight gain as M%. In seawater, both moisture and salt may be diffused into the composite and they increase the weight of the specimens after different time periods. Seawater absorption can influence impact and compressive strength. Factors such as the type of material, specimen diameter and length of exposure can affect the amount of seawater absorbed.

Glass/epoxy composite specimens which were cut from composites were immersed into seawater for periods of 3-, 6-, 9-, and 12-month. The rate of seawater absorption measured as the rate of weight change was determined. The changes of the absorbed moisture amount in seawater of the composite specimens according to seawater immersion time are given in Figure 4.1. It is seen that seawater immersion time increases the rate of weight gain as expected for each specimen diameter. Namely, the amount of moisture absorption increases up to 9-month wet condition and it has maximum value for each specimen diameter. After that it decreases as shown in the Figure 4.1.

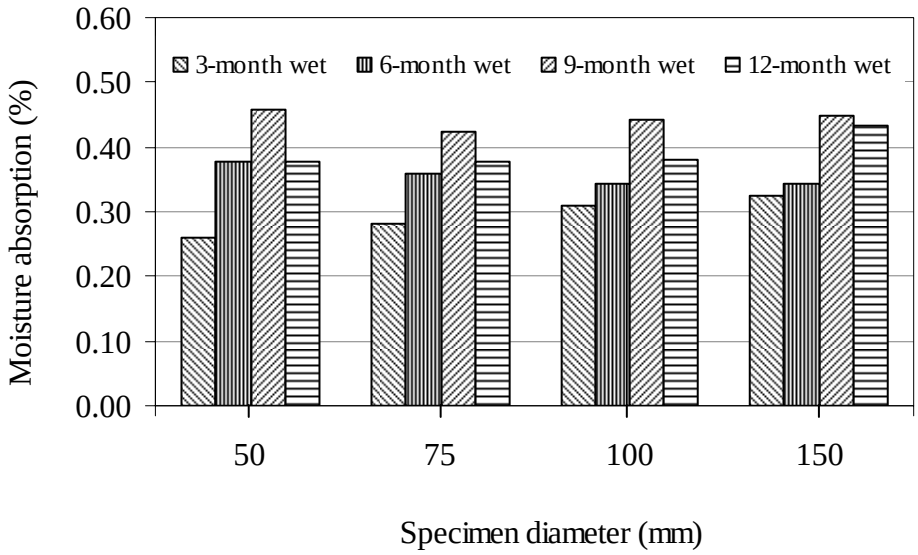

Figure 4.1 Amount of moisture absorption-specimen diameter diagram for different seawater immersion time

The changes of the moisture amount absorbed in seawater of the composite specimens having four different diameters are given in Figure 4.2. It is seen that as a percent absorbed of the moisture amount increases with increasing of specimen diameter for 3-month wet. In contrast, it decreases for 6-month wet with increasing specimen diameter.

The levels of maximum weight gain in seawater were recorded for 9-month immersion time. However the amount of moisture absorption slightly decreases at 12-month wet. The movement of seawater through a semipermeable membrane from inside of the specimen to outside seawater in order to equalize the osmotic pressure created by concentration differences. The behavior of osmosis may cause of decrease in the rate of moisture absorption with seawater immersion time. In similar a study, seawater uptake behavior has been observed by Kootsookos & Mouritz (2004) for glass/polyester and glass/vinyl ester composites.

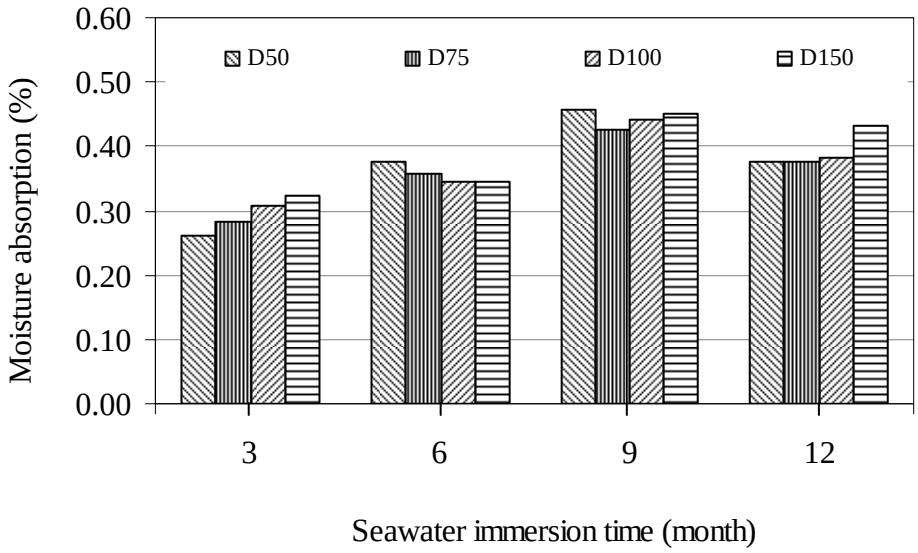

Figure 4.2 Amount of moisture absorption-seawater immersion time diagram for four different specimen diameters

The weight changes for each specimen's diameter are shown in below Tables. The results are listed in Table 4.1, Table 4.2, Table 4.3, and Table 4.4; for diameter 50, 75, 100, and 150 mm, respectively. The mean and the standard deviation of the seawater absorption were also calculated for all the specimens. Increasing the immersion time increases the rate of weight gain as expected. It is observed that the absorbed moisture increases with increasing of the time up to 9-month. After then absorbed amounts of moisture decreases. The moisture content evaluated for the different specimens are tabulated below

Table 4.1 Amounts of moisture absorption of diameter 50 mm composite specimens

Specimen No:	Seawater immersion time (Month)	Initial weight (g)	Final weight (g)	Moisture Absorbed (g)	Standard Deviation
1	3-month	79.225	79.455	0.230	**0.02**
2		77.700	77.900	0.200	
3		78.280	78.470	0.190	
4		78.580	78.780	0.200	
	Average	**78.446**	**78.651**	**0.205**	
1	6-month	80.125	80.355	0.230	**0.05**
2		78.850	79.190	0.340	
3		80.150	80.450	0.300	
4		77.500	77.820	0.320	
	Average	**79.16**	**79.45**	**0.295**	
1	9-month	82.350	82.680	0.330	**0.03**
2		80.723	81.090	0.368	
3		81.700	82.080	0.380	
4		80.250	80.660	0.410	
	Average	**81.256**	**81.628**	**0.372**	
1	12-month	78.300	78.645	0.345	**0.04**
2		79.200	79.460	0.260	
3		77.750	78.005	0.255	
4		77.900	78.220	0.320	
	Average	**78.288**	**78.583**	**0.295**	

Table 4.2 Amounts of moisture absorption of diameter 75 mm composite specimens

Specimen No:	Seawater immersion time (Month)	Initial weight (g)	Final weight (g)	Moisture Absorbed (g)	Standard Deviation
1	3-month	123.920	124.340	0.420	**0.06**
2		118.620	118.900	0.280	
3		127.400	127.740	0.340	
4		118.680	119.020	0.340	
	Average	**122.155**	**122.500**	**0.345**	
1	6-month	117.600	118.030	0.430	**0.01**
2		120.250	120.660	0.410	
3		122.400	122.840	0.440	
4		116.930	117.360	0.430	
	Average	**119.295**	**119.723**	**0.428**	
1	9-month	119.725	120.240	0.515	**0.02**
2		119.450	119.940	0.490	
3		123.800	124.300	0.500	
4		120.150	120.690	0.540	
	Average	**120.781**	**121.293**	**0.511**	
1	12-month	112.800	113.300	0.500	**0.11**
2		116.250	116.730	0.480	
3		112.300	112.575	0.275	
4		119.300	119.785	0.485	
	Average	**115.163**	**115.598**	**0.435**	

Table 4.3 Amounts of moisture absorption of diameter 100 mm composite specimens

Specimen No:	Seawater immersion time (Month)	Initial weight (g)	Final weight (g)	Moisture Absorbed (g)	Standard Deviation
1	3-month	165.550	166.030	0.480	**0.05**
2		157.260	157.820	0.560	
3		158.880	159.390	0.510	
4		168.350	168.800	0.450	
	Average	**162.510**	**163.010**	**0.500**	
1	6-month	166.850	167.420	0.540	**0.07**
2		160.700	161.270	0.570	
3		163.950	164.590	0.640	
4		151.750	152.220	0.470	
	Average	**160.813**	**161.368**	**0.555**	
1	9-month	157.200	157.760	0.560	**0.06**
2		157.600	158.240	0.640	
3		164.225	164.920	0.695	
4		159.925	160.560	0.635	
	Average	**159.738**	**160.370**	**0.632**	
1	12-month	185.600	186.360	0.760	**0.11**
2		154.300	154.930	0.630	
3		146.900	147.450	0.550	
4		149.600	150.100	0.500	
	Average	**159.100**	**159.710**	**0.610**	

Table 4.4 Amounts of moisture absorption of diameter 150 mm composite specimens

Specimen No:	Seawater immersion time (Month)	Initial weight (g)	Final weight (g)	Moisture Absorbed (g)	Standard Deviation
1	3-month	255.200	256.060	0.860	**0.08**
2		237.350	238.050	0.700	
3		249.700	250.550	0.850	
4		266.580	267.450	0.870	
	Average	**252.208**	**253.028**	**0.820**	
1	6-month	252.430	253.340	0.910	**0.03**
2		265.700	266.610	0.910	
3		245.180	246.030	0.850	
4		276.030	276.930	0.900	
	Average	**259.835**	**260.728**	**0.893**	
1	9-month	262.300	263.470	1.170	**1.65**
2		269.250	270.370	1.120	
3		269.450	270.610	1.160	
4		260.175	264.630	4.455	
	Average	**265.29**	**267.27**	**1.98**	
1	12-month	254.500	256.710	2.210	**0.58**
2		245.750	246.845	1.095	
3		265.450	266.590	1.140	
4		250.300	251.240	0.940	
	Average	**254.000**	**255.346**	**1.346**	

4.2 Impact Tests

Impact tests were conducted on at least four specimens for each experimental parameters (15, 20, and 25J impact energies and 50, 75, 100, and 150 mm diameters of specimens) and time periods (0-, 3-, 6-, 9-, and 12-month of seawater immersion). Absorbed energy (E_a), maximum contact force and maximum deflection are three important parameters to evaluate the impact behavior of composite pipes. Absorbed energy is the energy absorbed by the composite specimen through the impact event by formation of damage inside the specimen. Average values of above parameters were calculated and given in related figures following.

4.2.1 Impact Energy Effects on Impact Behavior of Specimens

Contact force-time histories of the specimen impacted at 15, 20, and 25J energies having 50 mm diameter for five different environmental conditions are given in Figure 4.3. It is seen that with increasing impact energy, contact force increases for five different environmental conditions. The force-time behavior of the specimens exposed to seawater for 3-month is different from that of other conditions. Because moisture absorption in 3-month is less than the others and the effect of salt of the seawater may be less than that of other environmental conditions.

Contact force versus contact time diagrams of specimens with 75, 100, 150 mm of diameters are shown in Figures 4.4-6. Contact force-time behaviors of these specimens are similar to that of 50 mm diameter specimen.

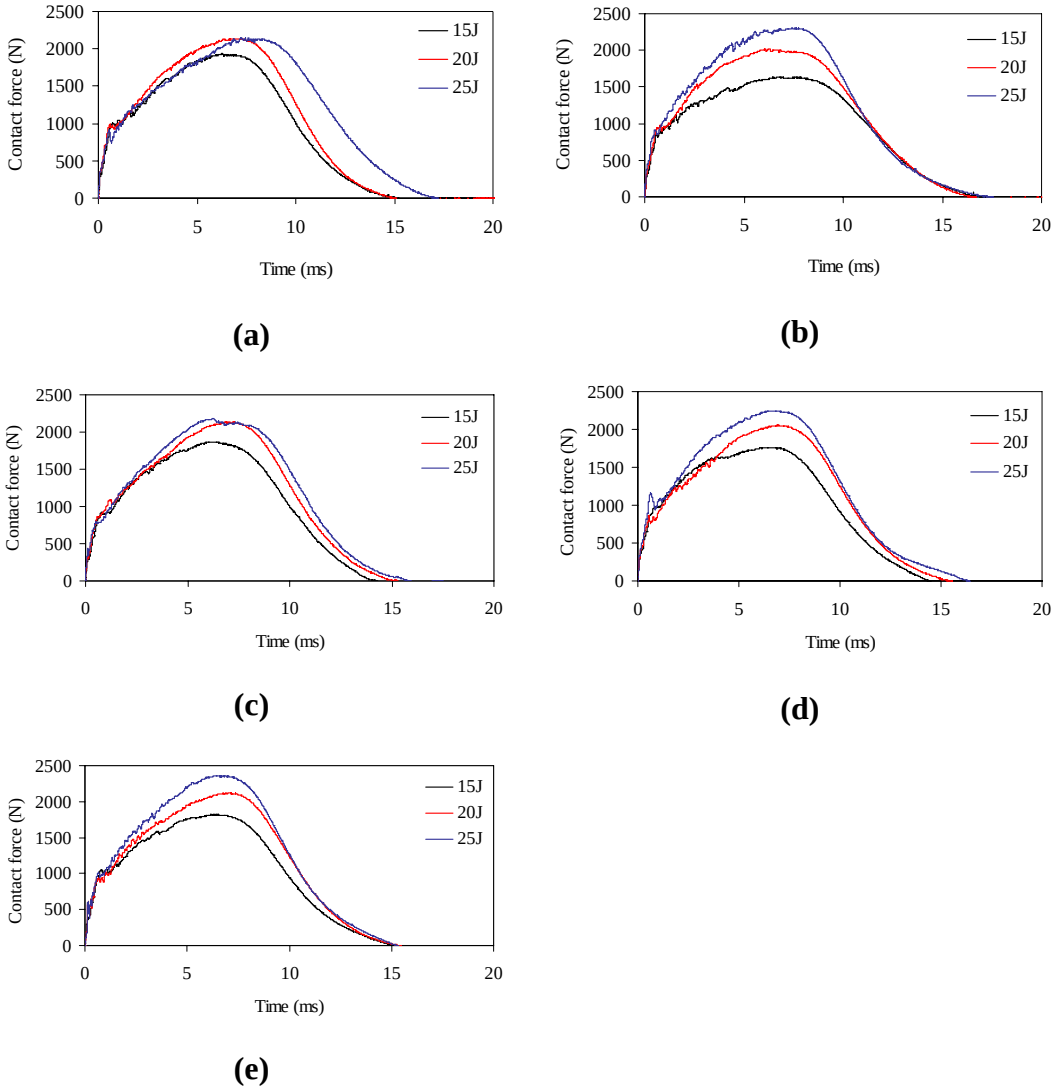

Figure 4.3 Contact force-time diagrams of the pipes having 50 mm diameter at **(a)** dry condition and immersed in seawater conditions for **(b)** 3-month, **(c)** 6-month, **(d)** 9-month, and **(e)** 12-month

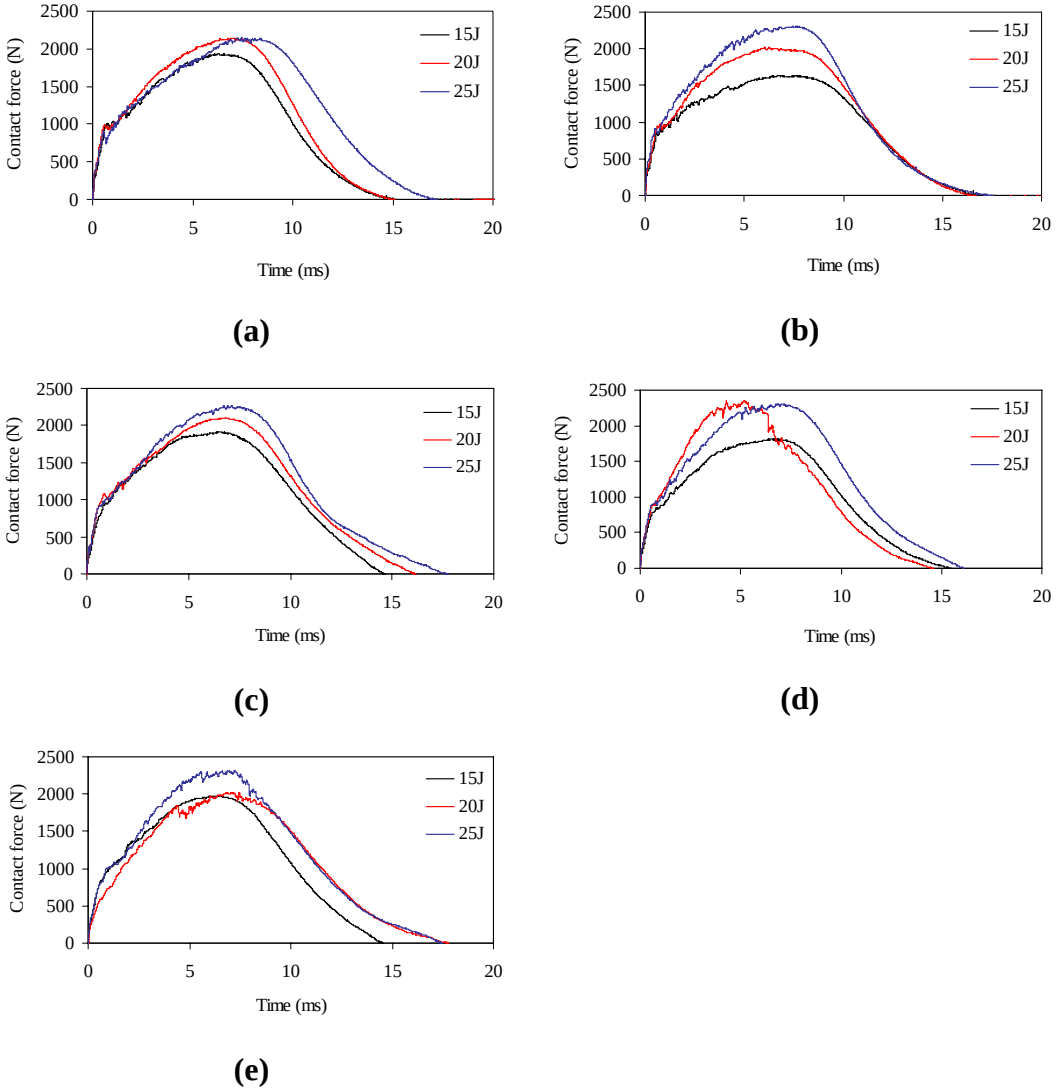

Figure 4.4 Contact force-time diagrams of the pipes having 75 mm diameter at **(a)** dry condition and immersed in seawater conditions for **(b)** 3-month, **(c)** 6-month, **(d)** 9-month, and **(e)** 12-month

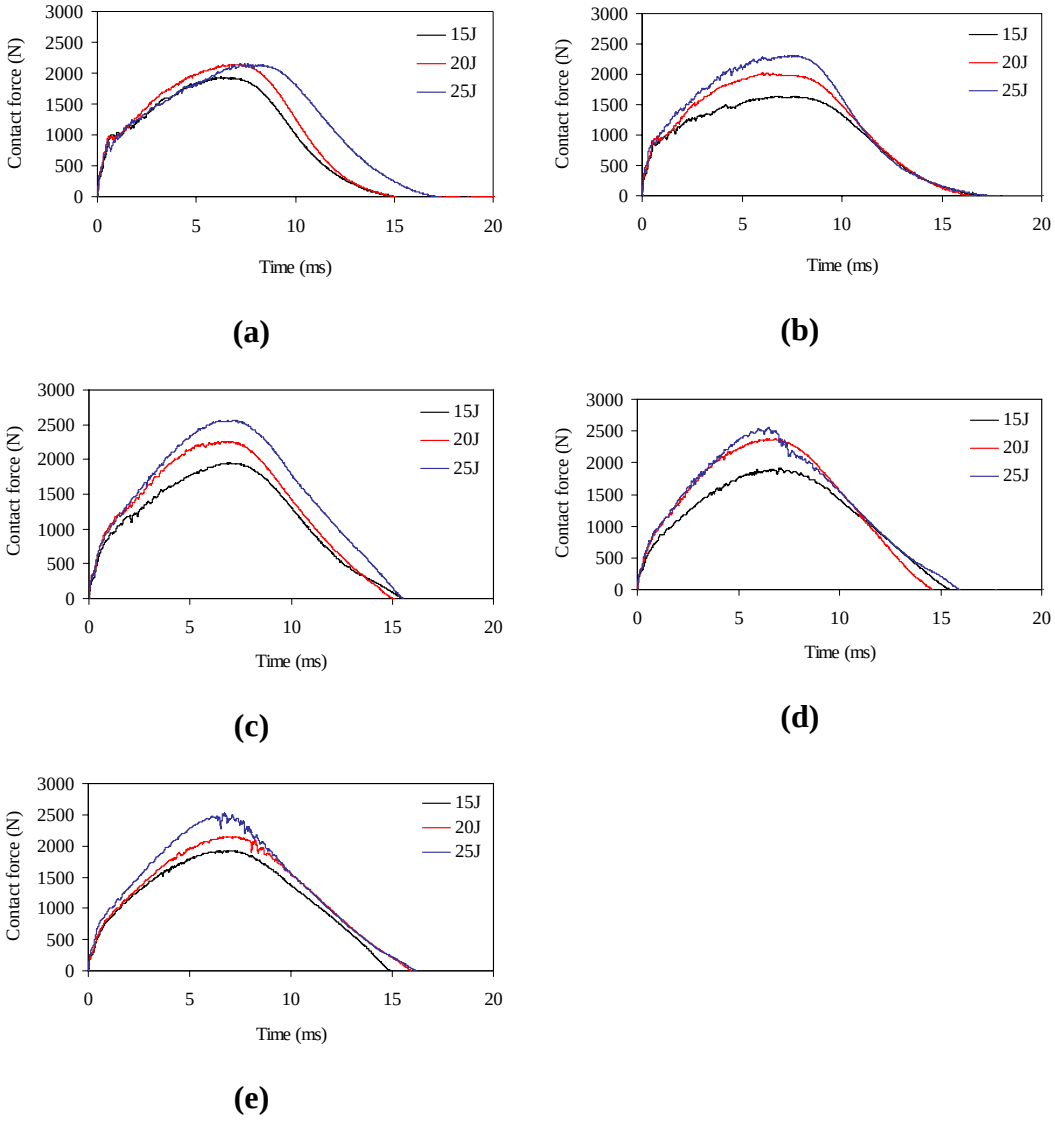

Figure 4.5 Contact force-time diagrams of the pipes having 100 mm diameter at **(a)** dry condition and immersed in seawater conditions for **(b)** 3-month, **(c)** 6-month, **(d)** 9-month, and **(e)** 12-month

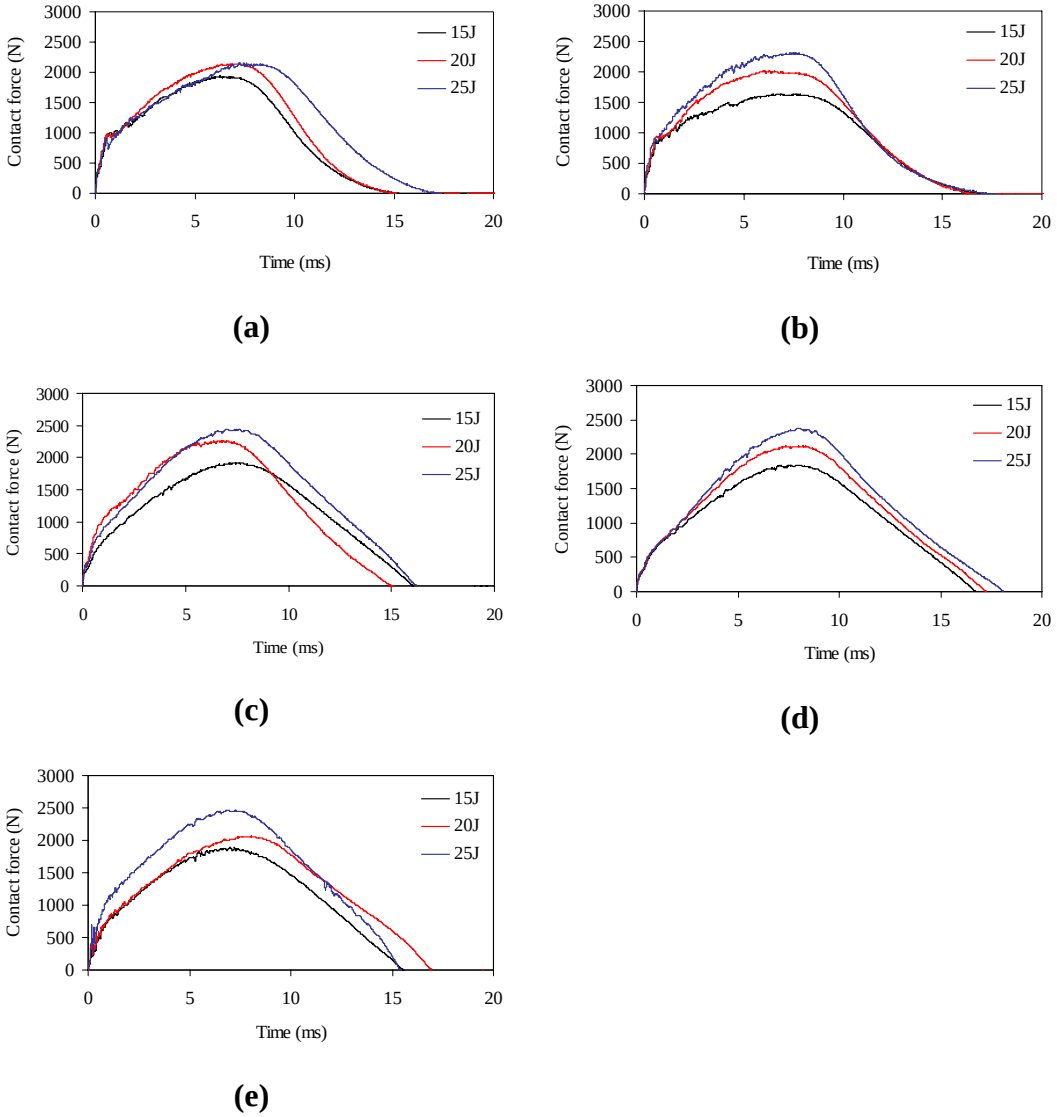

Figure 4.6 Contact force-time diagrams of the pipes having 150 mm diameter at **(a)** dry condition and immersed in seawater conditions for **(b)** 3-month, **(c)** 6-month, **(d)** 9-month, and **(e)** 12-month

Contact force-deflection diagrams of the pipes having 50 mm diameter at dry condition and immersed in seawater conditions are given in Figure 4.7. From the figure, it is seen that the maximum contact force and maximum deflection values increases by increasing the impact energy for all conditions. For all curves have two slopes, the first and the second. The second slope is smaller than first one because of the occurrence of failures such as matrix cracks, delaminations and fiber fractures in the specimens. At the end of the second part having the second slope, the unloading curves return toward the origin of the diagram indicating rebounding. All the curves

obtained from the tests in this study were rebounding case. The penetration or perforation of the striker to the composite pipe was not observed.

Contact force-deflection diagrams of the pipes having 75, 100, 150 mm diameters for dry condition and immersed in seawater conditions are given in Figures 4.8-10. All the curves have the similar character with the curves of 50 mm diameter pipes. However the difference between the first and the second slopes decrease with increasing the pipe diameter.

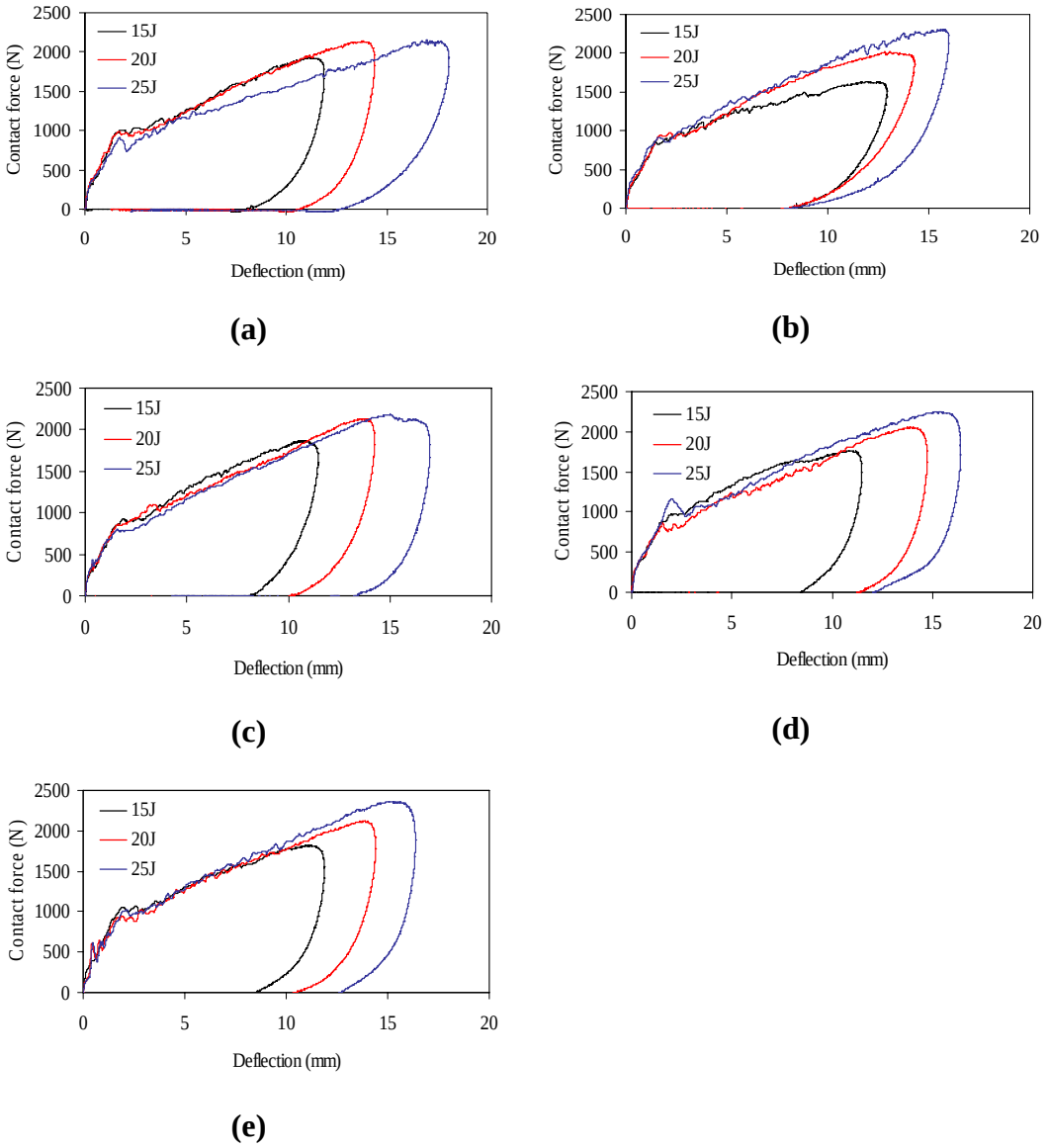

Figure 4.7 Contact force-deflection diagrams of the pipes having 50 mm diameter at **(a)** dry condition and immersed in seawater conditions for **(b)** 3-month, **(c)** 6-month, **(d)** 9-month, and **(e)** 12-month

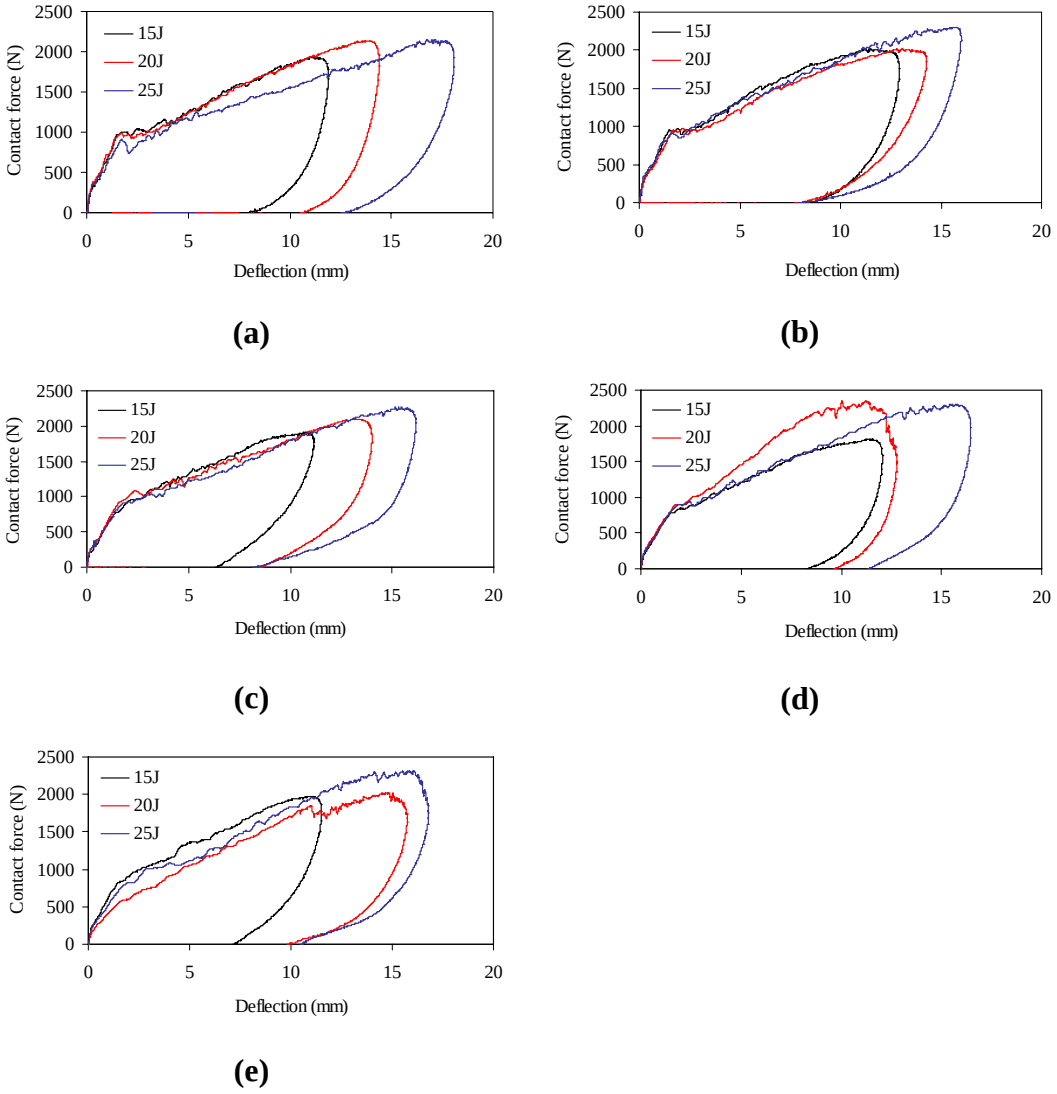

Figure 4.8 Contact force-deflection diagrams of the pipes having 75 mm diameter at **(a)** dry condition and immersed in seawater conditions for **(b)** 3-month, **(c)** 6-month, **(d)** 9-month, and **(e)** 12-month

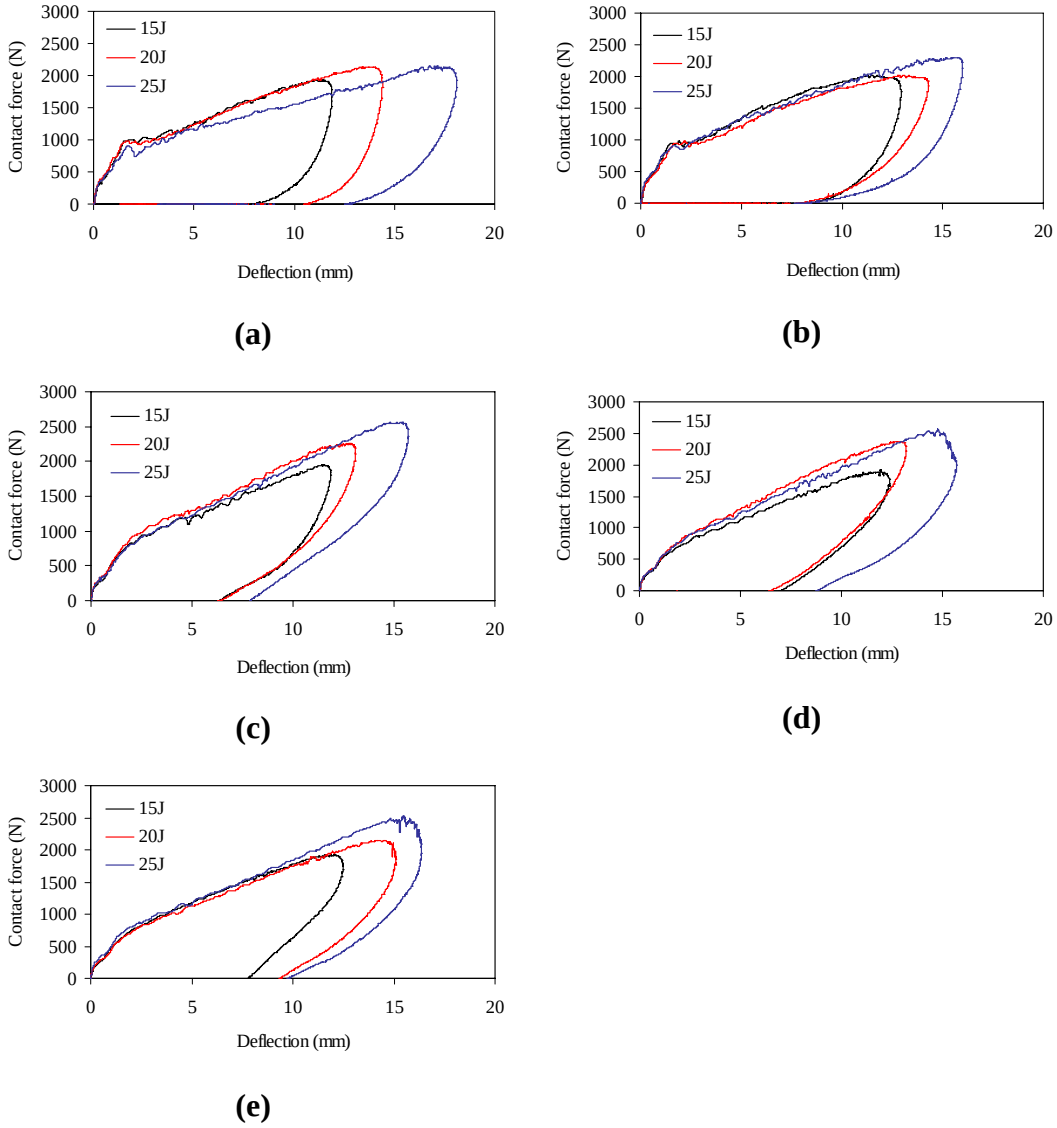

Figure 4.9 Contact force-deflection diagrams of the pipes having 100 mm diameter at **(a)** dry condition and immersed in seawater conditions for **(b)** 3-month, **(c)** 6-month, **(d)** 9-month, and **(e)** 12-month

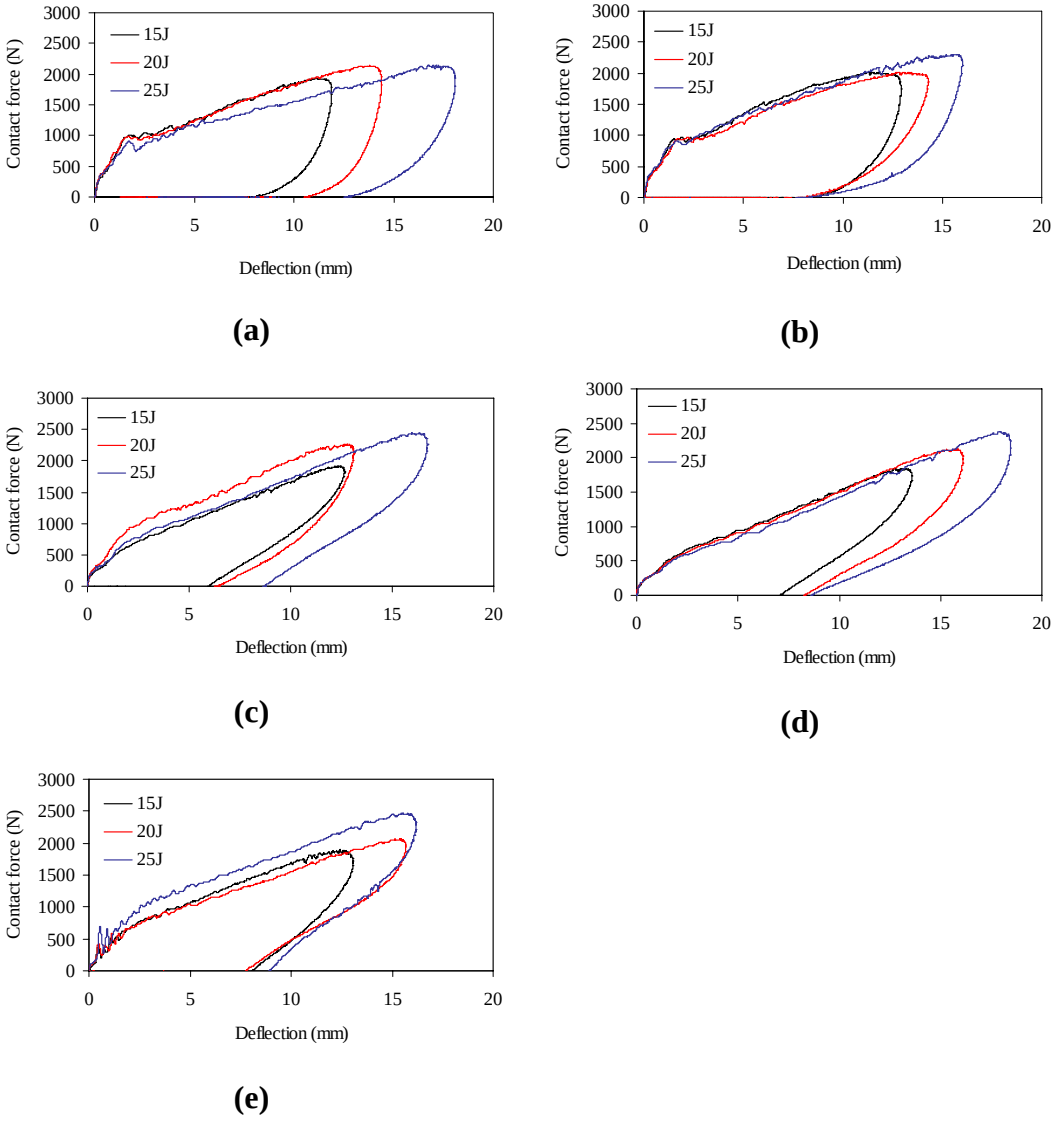

Figure 4.10 Contact force-deflection diagrams of the pipes having 150 mm diameter at **(a)** dry condition and immersed in seawater conditions for **(b)** 3-month, **(c)** 6-month, **(d)** 9-month, and **(e)** 12-month

4.2.2 Environmental Effects on Impact Behavior of Specimens

Discussion with contact force-deflection diagrams was made earlier for different impact energies. So in this part, environmental effects on contact force-deflection behavior will be discussed. Contact force-deflection behaviors of composite specimens are illustrated in Figure 4.11-14 for different seawater conditions, impact energies and specimen diameters. As can be seen from Figure 4.11, environmental conditions do not affect significantly on loading case of contact force-deflection diagrams. But environmental conditions have significant effect on unloading case. Because seawater erodes matrix with increasing seawater immersion time and different failures can occur in the composite specimen.

By increasing of specimen diameter, environmental conditions affect also on loading case of diagrams. In these specimens, impact failures are less than specimen with 50 mm diameter because of the more elastic behavior. Failure by eroding of seawater can affect more than that of impact.

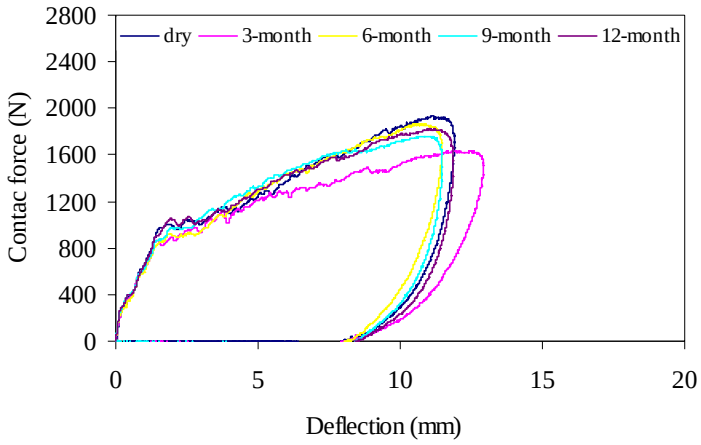

(a)

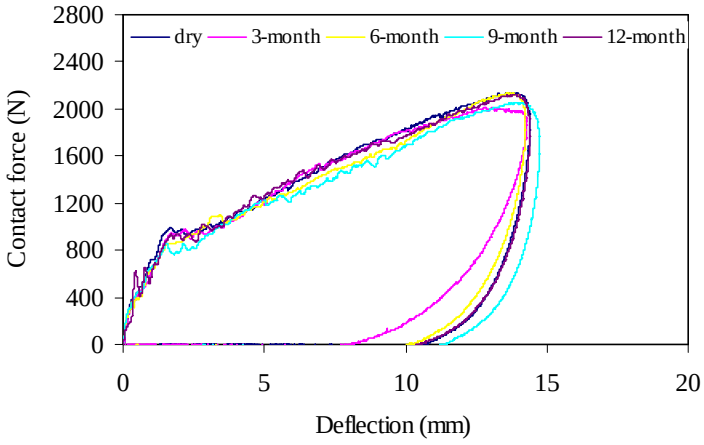

(b)

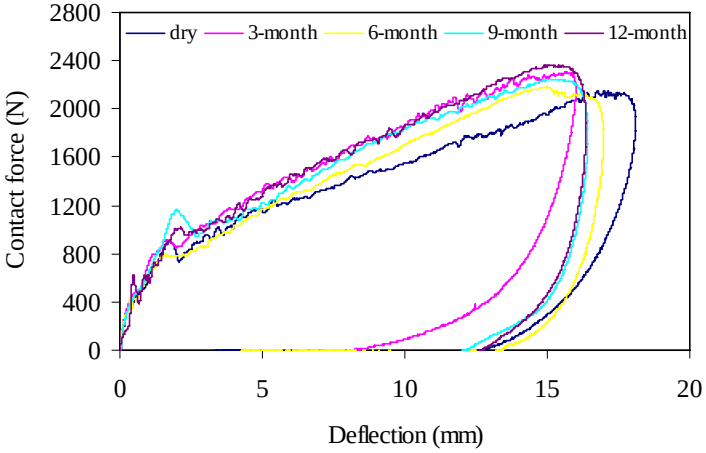

(c)

Figure 4.11 Contact force versus deflection curves of having 50 mm diameter composite pipes **(a)** 15J, **(b)** 20J, and **(c)** 25J

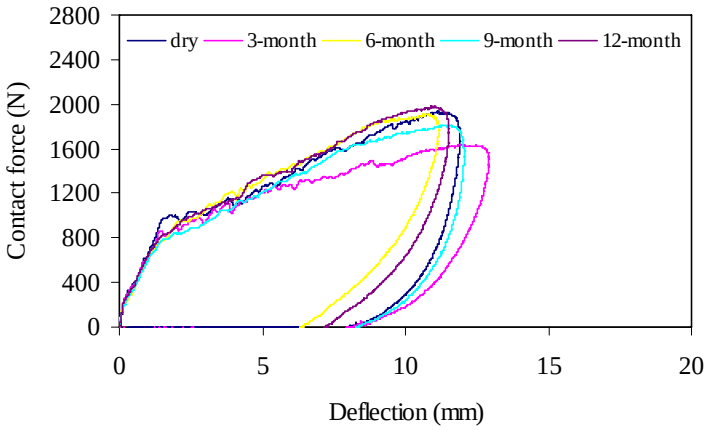

(a)

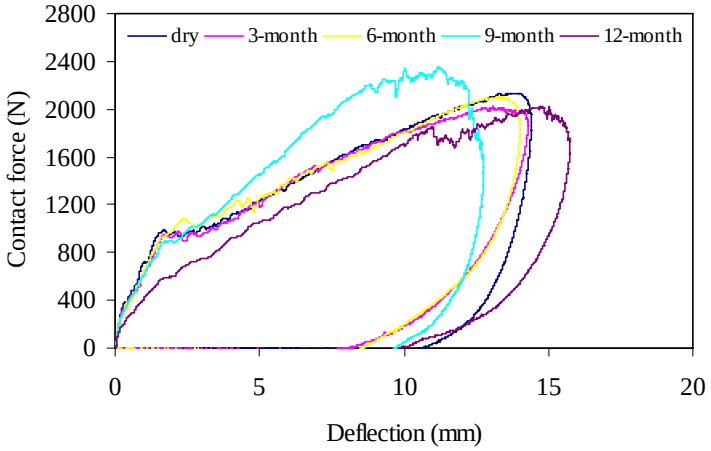

(b)

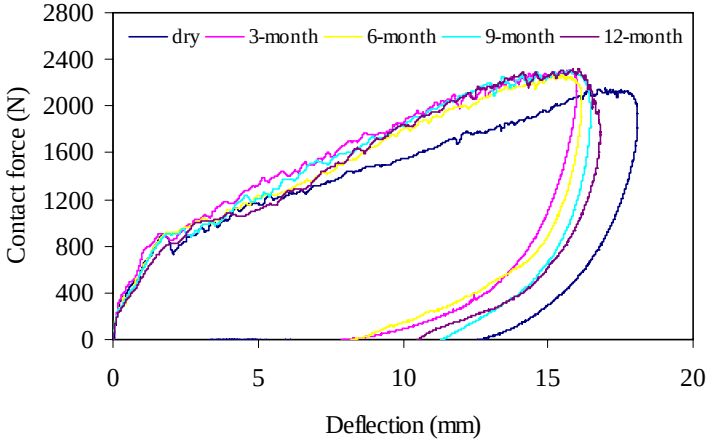

(c)

Figure 4.12 Contact force versus deflection curves of having 75 mm diameter composite pipes **(a)** 15J, **(b)** 20J, and **(c)** 25J

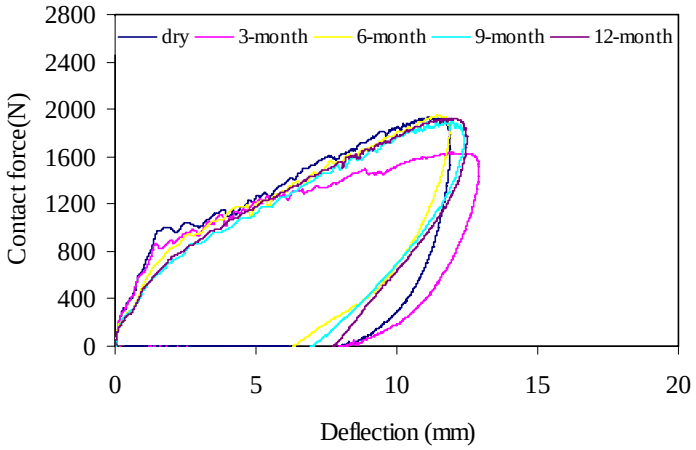

(a)

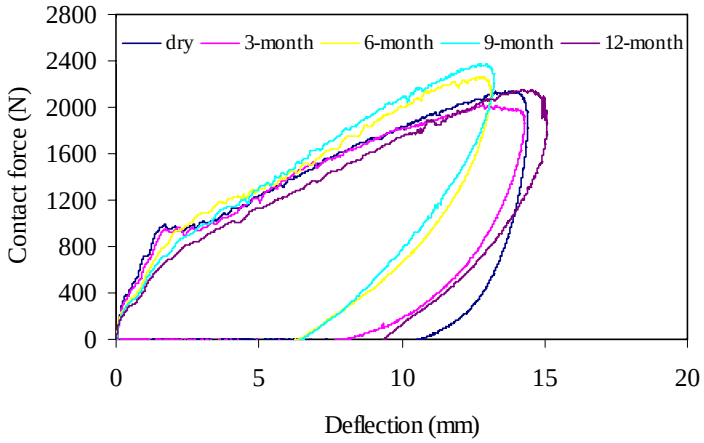

(b)

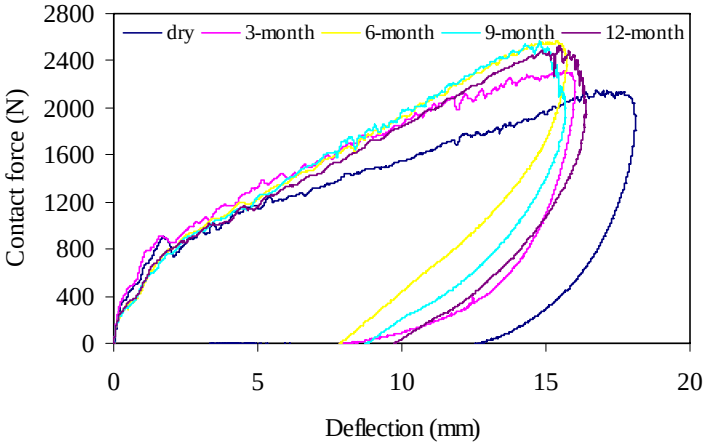

(c)

Figure 4.13 Contact force versus deflection curves of having 100 mm diameter composite pipes **(a)** 15J, **(b)** 20J, and **(c)** 25J

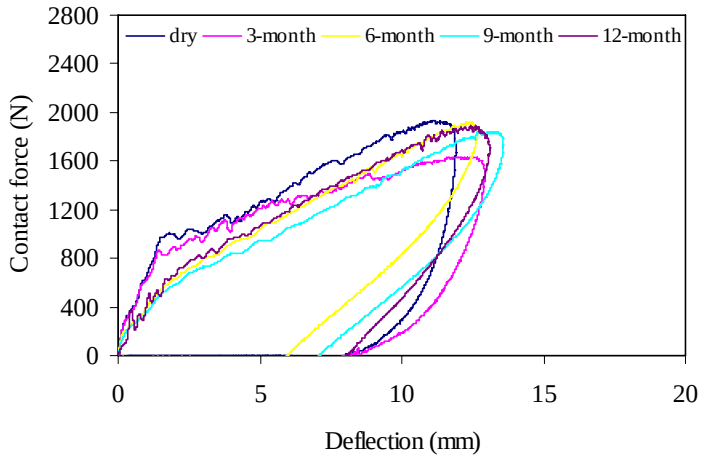

(a)

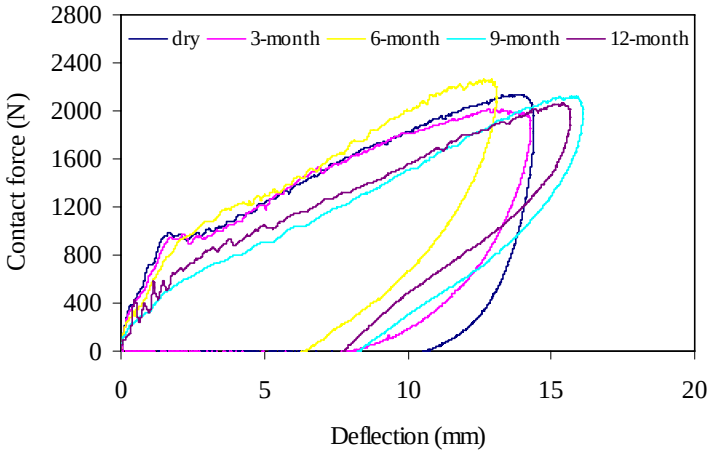

(b)

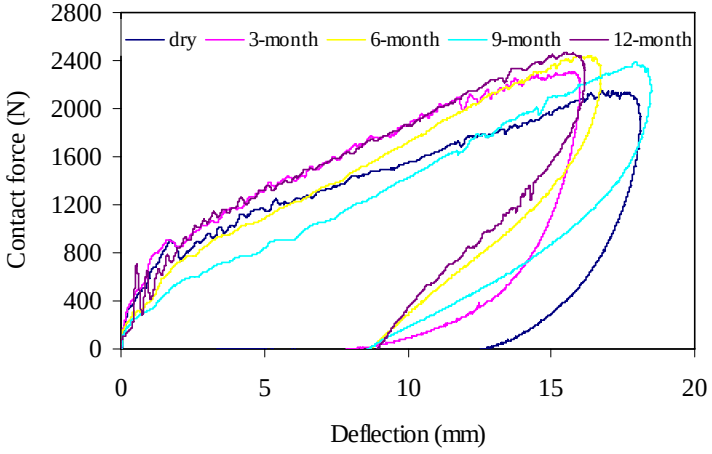

(c)

Figure 4.14 Contact force versus deflection curves of having 150 mm diameter composite pipes **(a)** 15J, **(b)** 20J, and **(c)** 25J

Figure 4.15 gives the maximum contact force-seawater immersion time curves of composite specimens with four different diameters for three impact energies. Dry condition is shown in the figure as 0 month immersed time. As can be seen that from figure for all diameters contact force increases by increasing the impact energy. Pipes having diameter-50 mm are little affected from seawater. However, for other pipes the contact force reaches the maximum value at third month immersed time and decline seen in the following months. As a result, not only the seawater immersion time, but also the diameter of the pipes and the impact energy affect the contact force between the composite specimens and the impactor nose.

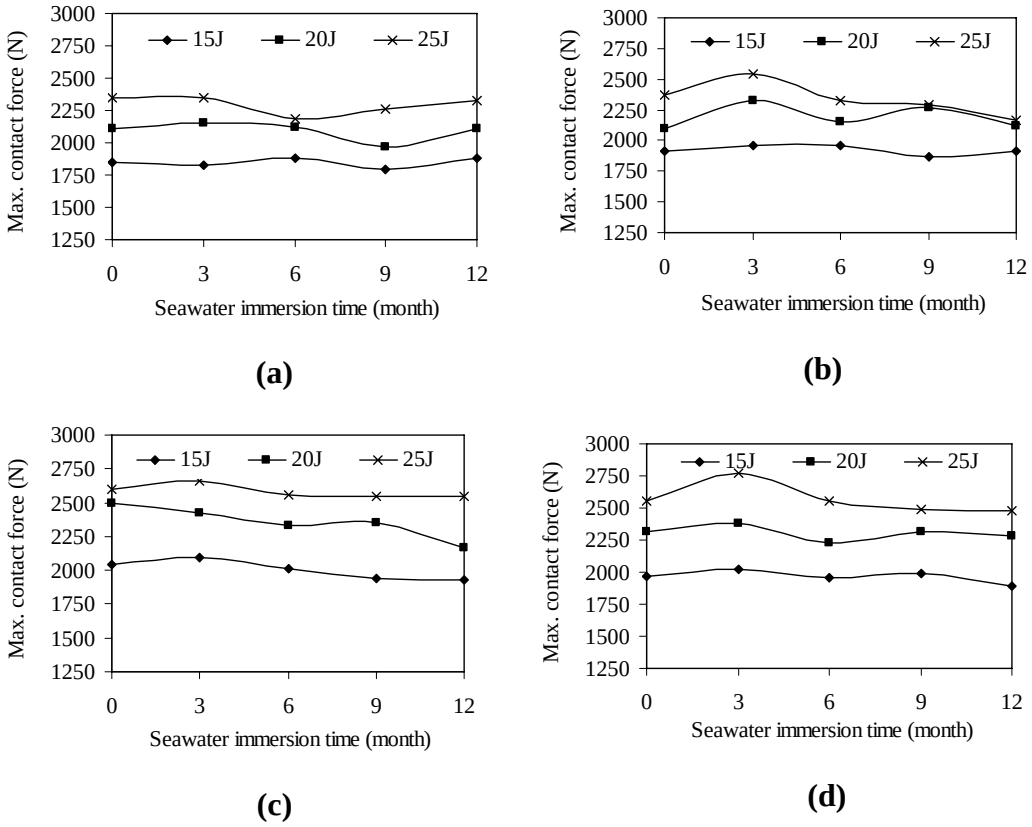

Figure 4.15 Contact force versus seawater immersion time curves of composite pipes with four different diameters of **(a)** 50 mm, **(b)** 75 mm, **(c)** 100 mm and **(d)** 150 mm

Elastic energy is the energy difference between the impact energy and the absorbed energy by the object causes the rebounding of the striker. As shown in the Figure 4.16, the energy absorbed by the pipe, the pipe diameter increases, decreases. That is, if the impact energy is held constant, the elastic energy increases with the

pipe diameter. In short, small-diameter pipes have great absorbed energy resulting in less strain energy. The energy absorbed by the sample is consumed for failure. As a result of this the failure area is larger for smaller diameter pipes (Figure 4.19-23). As can be seen in Figure 4.16, the absorbed energies of the pipes increase with increasing specimen diameter. It is also seen that at third month immersion time the absorbed energy by the pipes reaches the minimum value and than increases regularly.

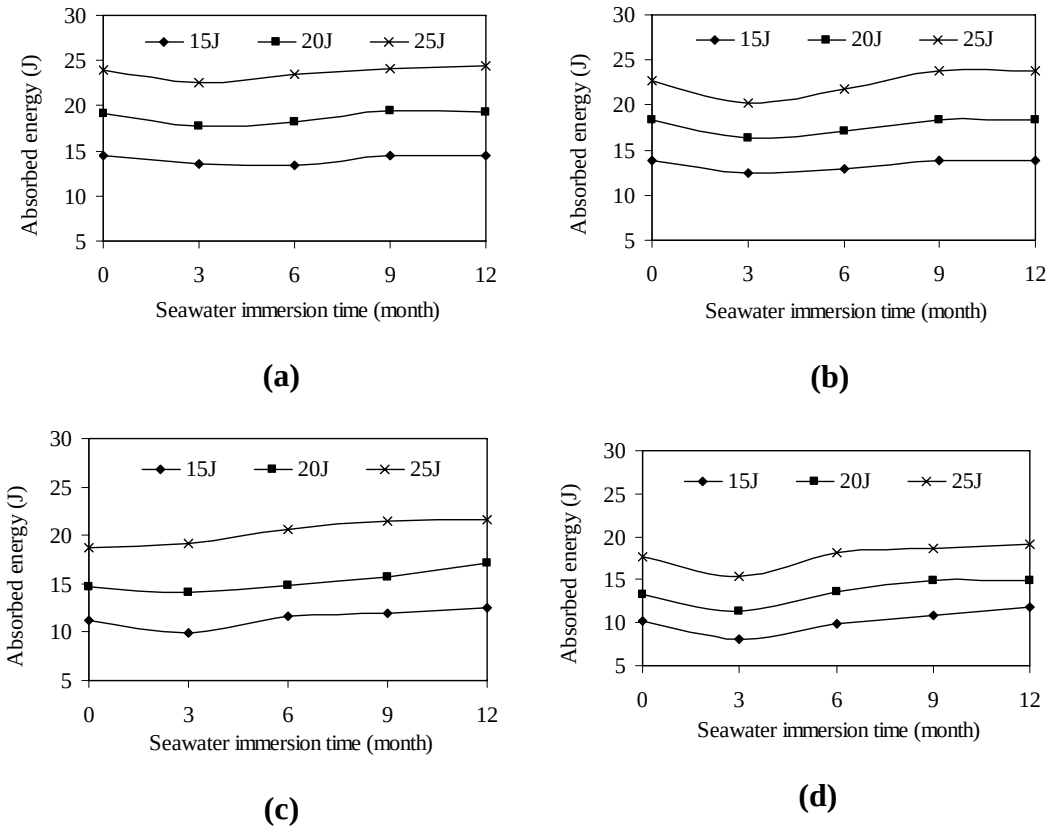

Figure 4.16 Absorbed energy versus seawater immersion time curves of composite pipes with four different diameters of **(a)** 50 mm, **(b)** 75 mm, **(c)** 100 mm, and **(d)** 150 mm

The maximum deflection can be defined as the magnitude of the movement of the impact point from non-impacted case to impacted case and is an important impact characteristic. Maximum deflection versus seawater immersion time curves of composite pipes for all diameters are given in Figure 4.17. For the all pipes, the deflection increases with increasing impact energy. Pipes having diameter-50 mm is

little affected from seawater. However, for other pipes the maximum deflection reaches the minimum value at third month immersed time and inclines seen in the following months' experiments.

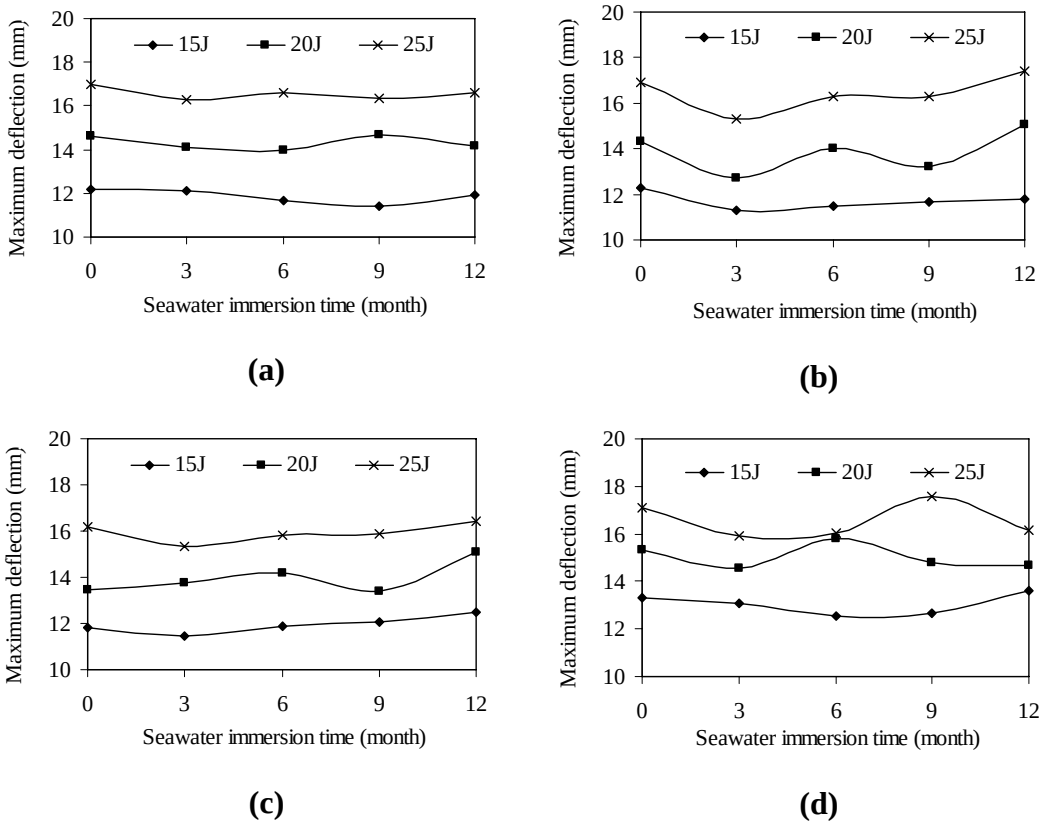

Figure 4.17 Maximum deflection versus seawater immersion time curves of composite pipes with four different diameters of **(a)** 50 mm, **(b)** 75 mm, **(c)** 100 mm, and **(d)** 150 mm

For each specimen diameter, for different impact energies contact time versus environmental conditions histories are given in Figure 4.18. Contact time is to be maximum in the specimen with 50 mm diameter exposed seawater at 3-month. After the 6-month, contact time is to be minimum for 15 and 20J impact energies while it does not change significantly for 25J impact energy.

For 75 mm diameter, contact time decreases with increasing of seawater immersion time for 15J impact energy. It shows fluctuating behavior according to the seawater immersion time for other energies. For 100 mm diameter, contact time does not change significantly with immersion time while it behaves wavy. In the specimen

with 150 mm diameter, contact time curves follow each other by the phase difference.

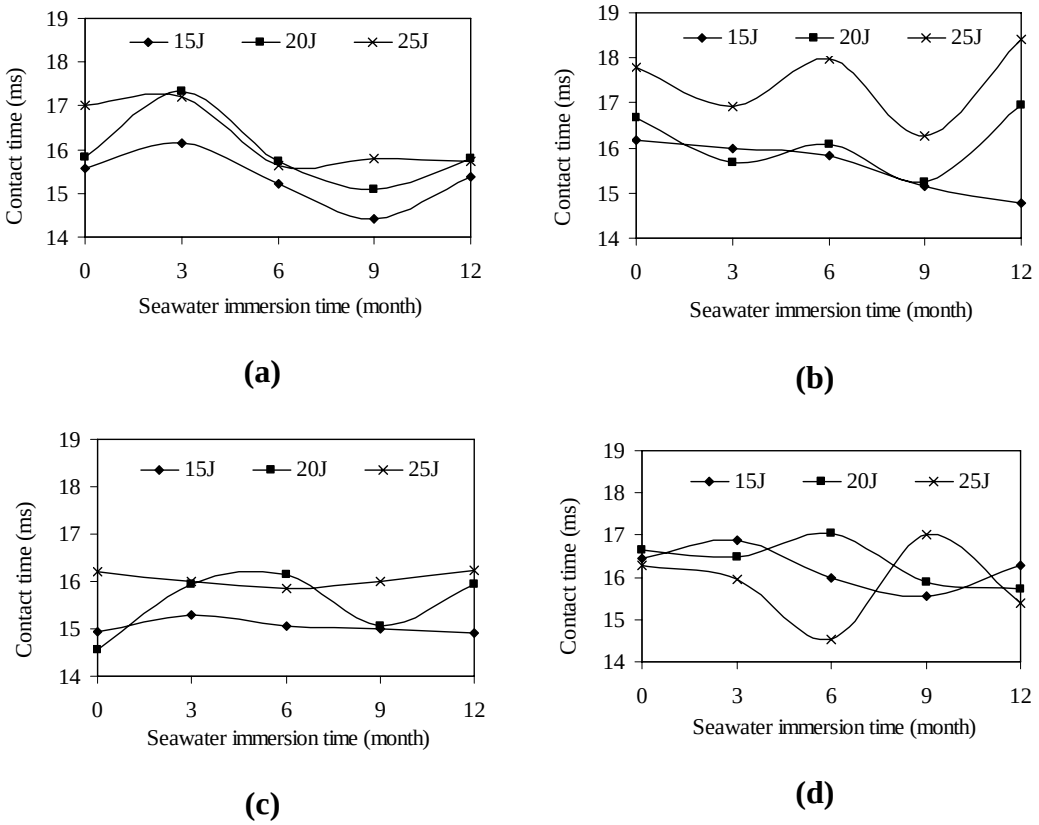

Figure 4.18 Contact time versus seawater immersion time curves of composite pipes with four different diameters of **(a)** 50 mm, **(b)** 75 mm, **(c)** 100 mm, and **(d)** 150 mm

4.2.3 Damages of Composite Specimens

To explain the damage case of the composite pipes, damage images of the impacted (at impact energies as 15J, 20J, and 25J) specimens having 50 mm, 75 mm, 100 mm, and 150 mm diameters and for each environmental condition (dry, 3-, 6-, 9-, and 12-month seawater immersed time) are given in Figure 4.19-23.

Figures give the damages around the impact points of the specimens during immersed time. Matrix cracks, delaminations and fiber failure can be seen in this figure. As can be seen from figures in the lower specimen diameters, the delamination pattern is dependent upon the structure of the fabric such as winding angle. Butterfly shape with diagonal lines parallel to the fiber directions was observed in the impacted composite pipes. Especially for pipe specimens having lower diameter, the delamination areas increase with increasing impact energy. It is also seen that the delamination areas increase dramatically with decreasing specimen diameter. Because, the pipe specimens having larger diameter are more flexible, have more elastic energy and less absorbed energy for failure.

15J 20J 25J

(a)

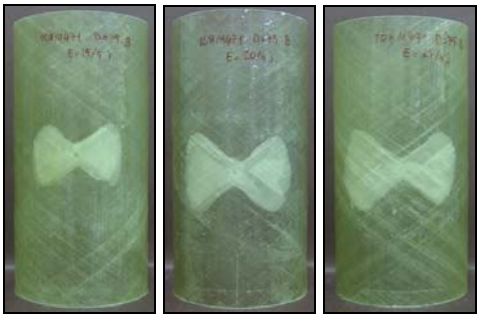

15J 20J 25J

(b)

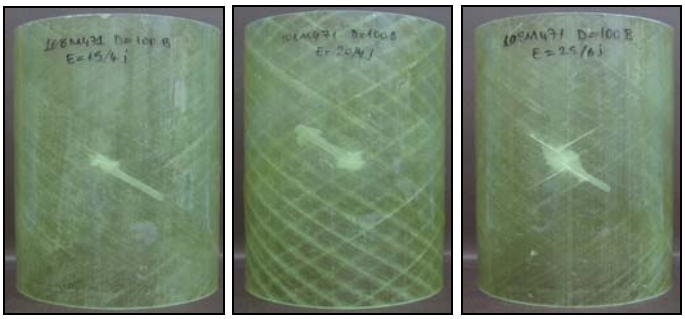

15J 20J 25J

(c)

15J 20J 25J

(d)

Figure 4.19 Damages around the impact points of the pipes for dry case **(a)** diameter 50 mm, **(b)** diameter 75 mm, **(c)** diameter 100 mm, and **(d)** diameter 150 mm

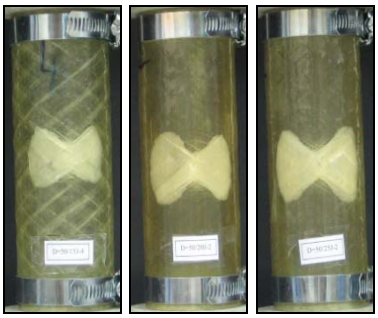

15J 20J 25J

(a)

15J 20J 25J

(b)

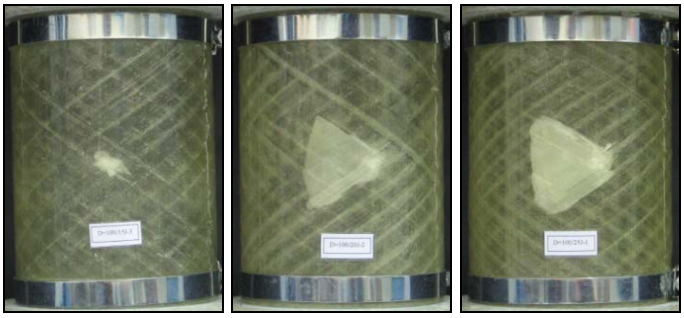

15J 20J 25J

(c)

15J 20J 25J

(d)

Figure 4.20 Damages around the impact points of the pipes immersed in seawater during 3-month **(a)** diameter 50 mm, **(b)** diameter 75 mm, **(c)** diameter 100 mm, and **(d)** diameter 150 mm

15J 20J 25J

(a)

15J 20J 25J

(b)

15J 20J 25J

(c)

15J 20J 25J

(d)

Figure 4.21 Damages around the impact points of the pipes immersed in seawater during 6-month **(a)** diameter 50 mm, **(b)** diameter 75 mm, **(c)** diameter 100 mm, and **(d)** diameter 150 mm

15J 20J 25J

(a)

15J 20J 25J

(b)

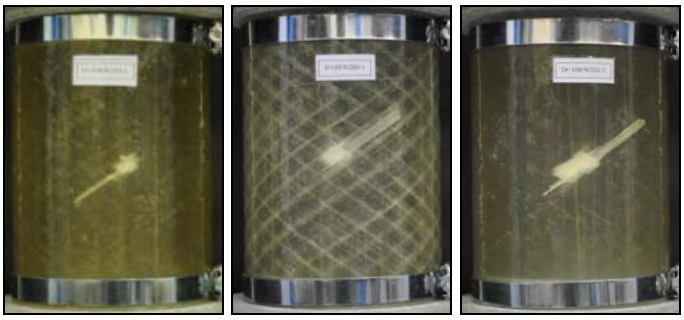

15J 20J 25J

(c)

15J 20J 25J

(d)

Figure 4.22 Damages around the impact points of the pipes immersed in seawater during 9-month **(a)** diameter 50 mm, **(b)** diameter 75 mm, **(c)** diameter 100 mm, and **(d)** diameter 150 mm

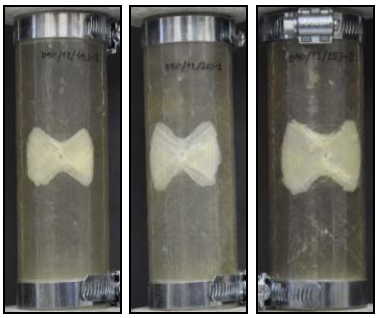

15J 20J 25J

(a)

15J 20J 25J

(b)

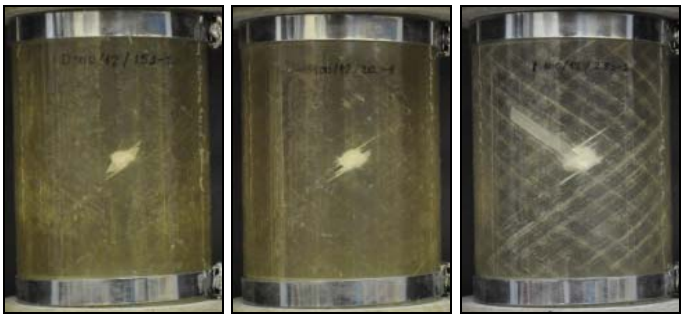

15J 20J 25J

(c)

15J 20J 25J

(d)

Figure 4.23 Damages around the impact points of the pipes immersed in seawater during 12-month **(a)** diameter 50 mm, **(b)** diameter 75 mm, **(c)** diameter 100 mm, and **(d)** diameter 150 mm

4.3 Axial Compression Test

Composite specimens were tested to characterize their compressive performance. The axial compression after impact test is an experimental estimation of reduction of the compressive strength of the composite pipes subjected to impact loading and environmental conditions.

In this part, axial compression results after impact test are evaluated. For all environmental conditions and specimen diameters, impacted and non-impacted specimens were subjected to axial compression loading. In here, the main aim is to examine the change of axial compression strength after impact of four different diameter specimens according to seawater immersion time.

The photos of having 50, 75, 100, and 150 mm diameters impacted and non-impacted specimens for dry condition subjected to compressive loading are given in Figure 4.24. It is seen that under axial compression load, specimen with 50 and 75 mm diameters shows reflect the rigid behavior. So buckling failure does not occur due to axial compression load. In the non-impacted specimens; compression damage starts from middle of the specimen clearly and then moves in the direction of fiber. But in the impacted specimens, compression damage was expands on impacted zone namely at middle of the specimen (Figure 4.24-a, b).

As can be seen from Figure 4.24-c, d, in the non-impacted specimens having 100 mm and 150 mm diameters, generally occur near the end of the specimen compression damages as the local buckling. Compressive damage generally occurs at the impacted specimens with 100 mm diameter and propagates from impact point with increasing impact energy (Figure 4.24-c). But in the specimens having 150 mm diameter, impact energy does not have effect on compressive behavior. Compressive failure occurs by buckling (Figure 4.24-d).

After waiting 3-month in seawater, impacted and non-impacted specimens having four different diameters are subjected to axial compression loading. Damaged

specimens are given in Figure 4.25. As shown in the figure, compressive failure occur the edge of the non-impacted specimens as the specimen diameter increases. Failure mode is the buckling. In the impacted specimens except for specimen with 150 mm diameter, compression damage usually initiates from the impacted zone and propagates in the direction of fiber.

In the specimens exposed seawater at 6-month, compression damages are presented in Figure 4.26. As can be seen from figure, compression damage occurs near the end of the non-impacted specimens as the local buckling. However, in the impacted specimen, compressive damage initiates from impact point and propagates with increasing impact energy (Figure 4.26-a, b, c). In the impacted specimens having 150 mm diameters, compression damage occurs by buckling (Figure 4.26-d).

Images of compression damage of the tested specimens after 9-month seawater immersion time are given Figure 4.27. As can be seen from the images, the compression damage except for the specimens with 50 mm diameter occurs near the end of the non-impacted specimens because of the local buckling. In the impacted specimens having the 50 mm and 75 mm diameters, compression damage initiates from impact point and progresses in the direction of fiber. But, this damage in the specimens having the 100 mm diameter changes impact zone damage from buckling at the end of the specimen by increasing of impact energy. In the 150 mm diameter specimens, failure takes place by buckling and impact region damage together. As seen in Figure 4.28, in all the non-impacted specimens immersed seawater at 12-month, dominant failure type is the buckling. In non-impacted specimens, compression damage as the local buckling occurred. In the impacted specimens having the 50 mm and 75 mm diameters, compressive damage was initiated from impact zone and propagated in the direction of fiber (Figure 4.28-a, b). However, in the impacted specimens having the 100 mm diameter, compression damage initiated by the buckling and then this damage progressed from impact point (Figure 4.28-c). In the 150 mm diameter specimens, dominant damage is the buckling. In addition to this damage, compression damage which follows impact damage occurs by increasing of impact energy (Figure 4.28-d).

0J 15J 20J 25J

(a)

0J 15J 20J 25J

(b)

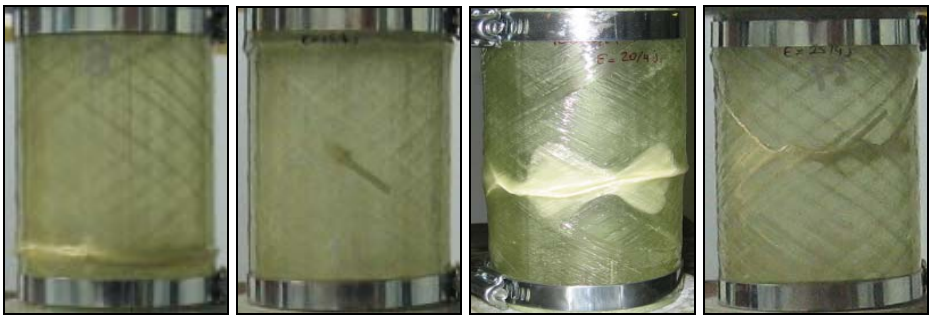

0J 15J 20J 25J

(c)

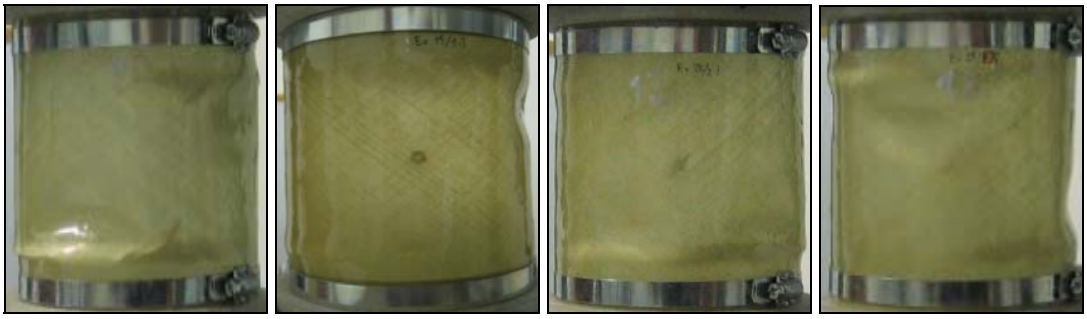

0J 15J 20J 25J

(d)

Figure 4.24 Images of the composite specimens subjected to axial compression after impact at dry condition for diameters **(a)** 50 mm, **(b)** 75 mm, **(c)** 100 mm, and **(d)** 150 mm

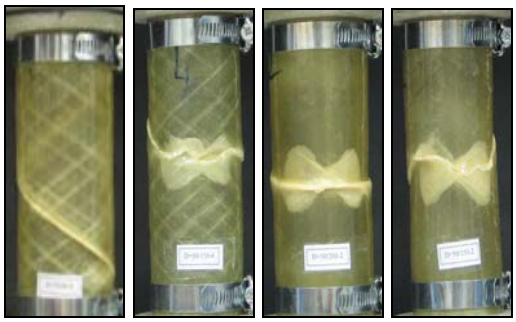

0J 15J 20J 25J

(a)

0J 15J 20J 25J

(b)

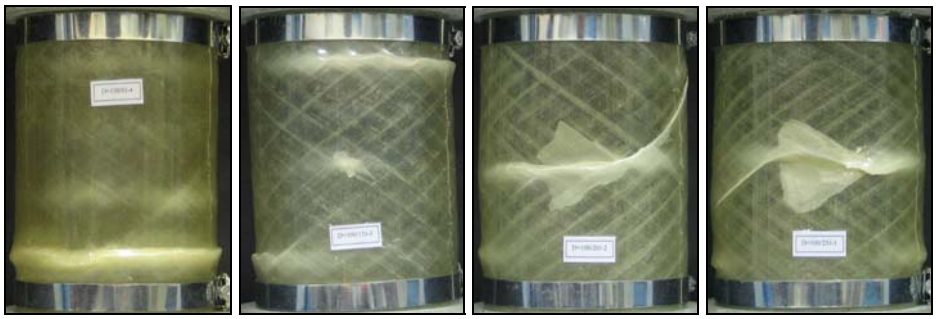

0J 15J 20J 25J

(c)

0J 15J 20J 25J

(d)

Figure 4.25 Images of the composite specimens subjected to axial compression after impact at 3-month seawater immersion condition for diameters **(a)** 50 mm, **(b)** 75 mm, **(c)** 100 mm, and **(d)** 150 mm

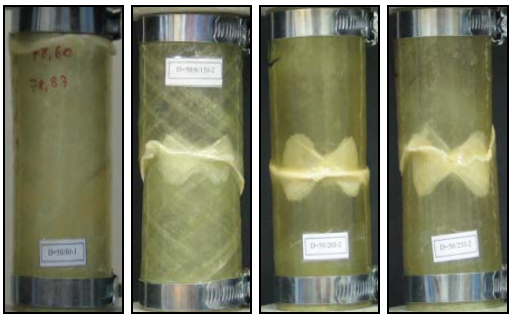

0J 15J 20J 25J

(a)

0J 15J 20J 25J

(b)

0J 15J 20J 25J

(c)

0J 15J 20J 25J

(d)

Figure 4.26 Images of the composite specimens subjected to axial compression after impact at 6-month seawater immersion condition for diameters **(a)** 50 mm, **(b)** 75 mm, **(c)** 100 mm, and **(d)** 150 mm

0J 15J 20J 25J

(a)

0J 15J 20J 25J

(b)

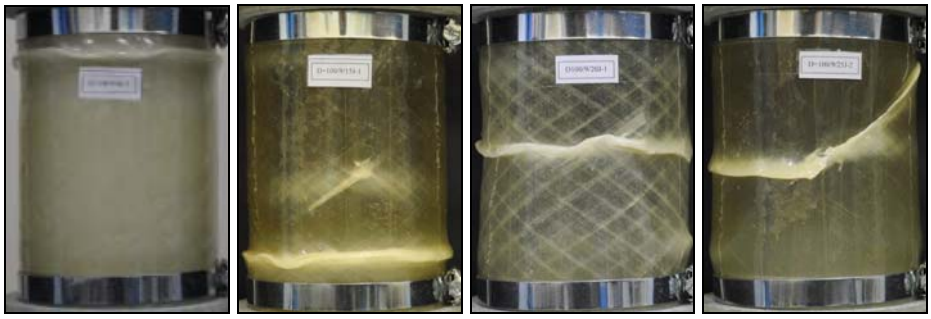

0J 15J 20J 25J

(c)

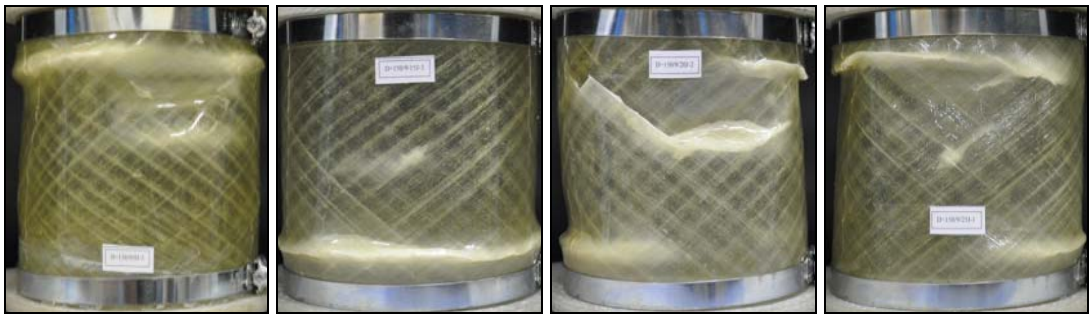

0J 15J 20J 25J

(d)

Figure 4.27 Images of the composite specimens subjected to axial compression after impact at 9-month seawater immersion condition for diameters **(a)** 50 mm, **(b)** 75 mm, **(c)** 100 mm, and **(d)** 150 mm

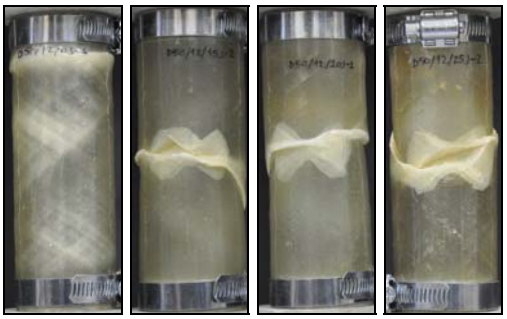

0J 15J 20J 25J

(a)

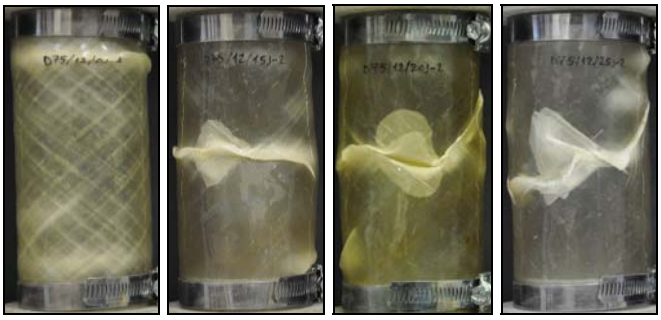

0J 15J 20J 25J

(b)

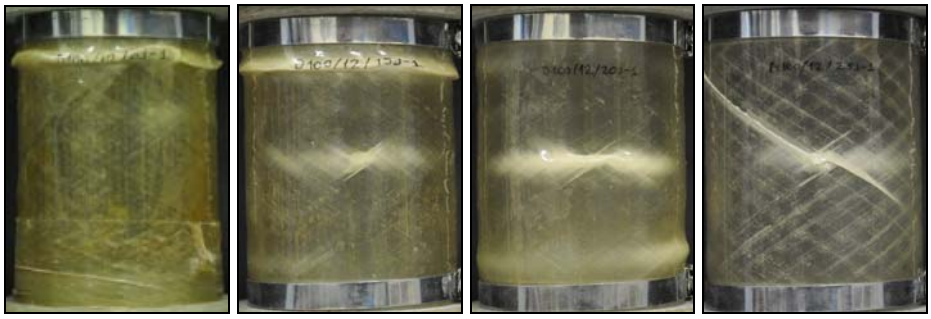

0J 15J 20J 25J

(c)

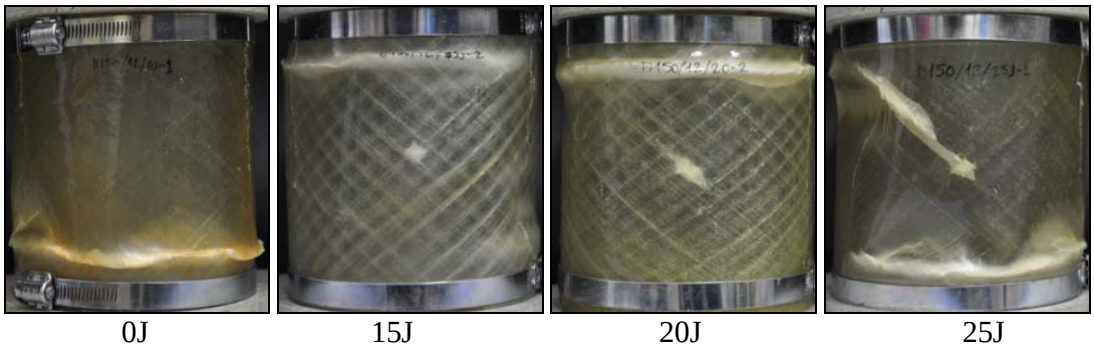

0J 15J 20J 25J

(d)

Figure 4.28 Images of the composite specimens subjected to axial compression after impact at 12-month seawater immersion condition for diameters **(a)** 50 mm, **(b)** 75 mm, **(c)** 100 mm, and **(d)** 150 mm

Compressive strength of composite specimens was determined before and after impact for different diameters and environmental conditions.

For the specimens with different diameters, the compressive strength versus seawater immersion time is given in Figure 4.29. For non-impacted case, compressive strength generally reduces with increasing seawater immersed time in the having 50, 75 and 100 mm diameter specimens. As given in Figure 4.29-a. For 150 mm diameter specimen, the situation is different a little and the compressive strength due to buckling demonstrates an alternating changeable situation. In all of the impacted specimen diameters, effect of seawater on compressive strength with increasing impact energy has decreased.

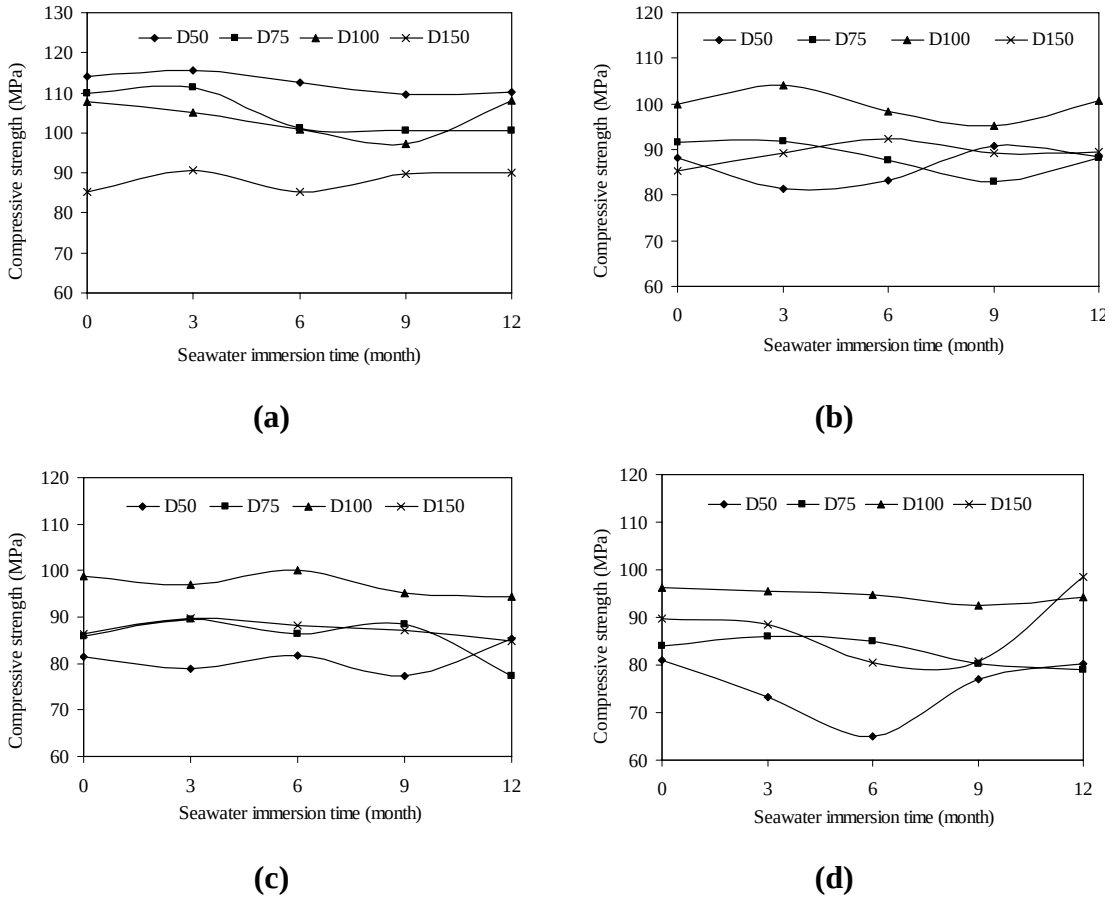

Figure 4.29 The compressive strength versus seawater immersion time for different impact energies **(a)** 0J, **(b)** 15J, **(c)** 20J, and **(d)** 25J

Maximum compressive strength occurs at the specimen with 100 mm diameter for all seawater immersion times and impact energies except for 12-month and 25J

impact energy while it exists at specimens with 50 mm diameter for non-impacted cases. Minimum compressive strength occurs generally at the specimens with 50 mm diameter for all environmental conditions because of the more impact failures, while it occurs at 150 mm diameter for non-impacted cases. Compressive strength shows similar behavior in the specimens with 50 and 100 mm diameter for non-impacted cases (Figure 4.29-a), and 75 mm and 100 mm for 15J impact energies (Figure 4.29-b). In generally, there is no significant effect of seawater immersion time on compressive strength. However, at 25 J impact energy, seawater immersion time has significant effect on compressive strength for the specimen with 50 mm diameter immersed seawater at 6-month and with 150 mm diameter at 12-month (Figure 4.29-d).

For the non-impacted and impacted specimens having different diameters, compressive strength versus seawater immersion time curves is given Figure 4.30. As can be seen from the figure, differences in compressive strengths between non-impacted specimens decrease by increasing of specimen's diameter. It means failures by impact and compression-after impact decrease by specimen diameter. Compressive strength decreases by increasing of seawater immersion time for 75 mm diameter. In the specimens having 50 and 75 mm diameters compressive strength generally decreases by increasing impact energy. In the 100 mm diameter specimen due to buckling, the compression strength shows an unstable dispersion. In specimens with the largest diameter, in case of the increasing the energy of impact, compressive strength has little affected from the seawater. In the non-impacted specimens, compressive strength of the 75 mm diameter specimen is mostly affected by seawater for all diameters and all impact energies. There is no significant change in the compressive strength between 9-12 months.

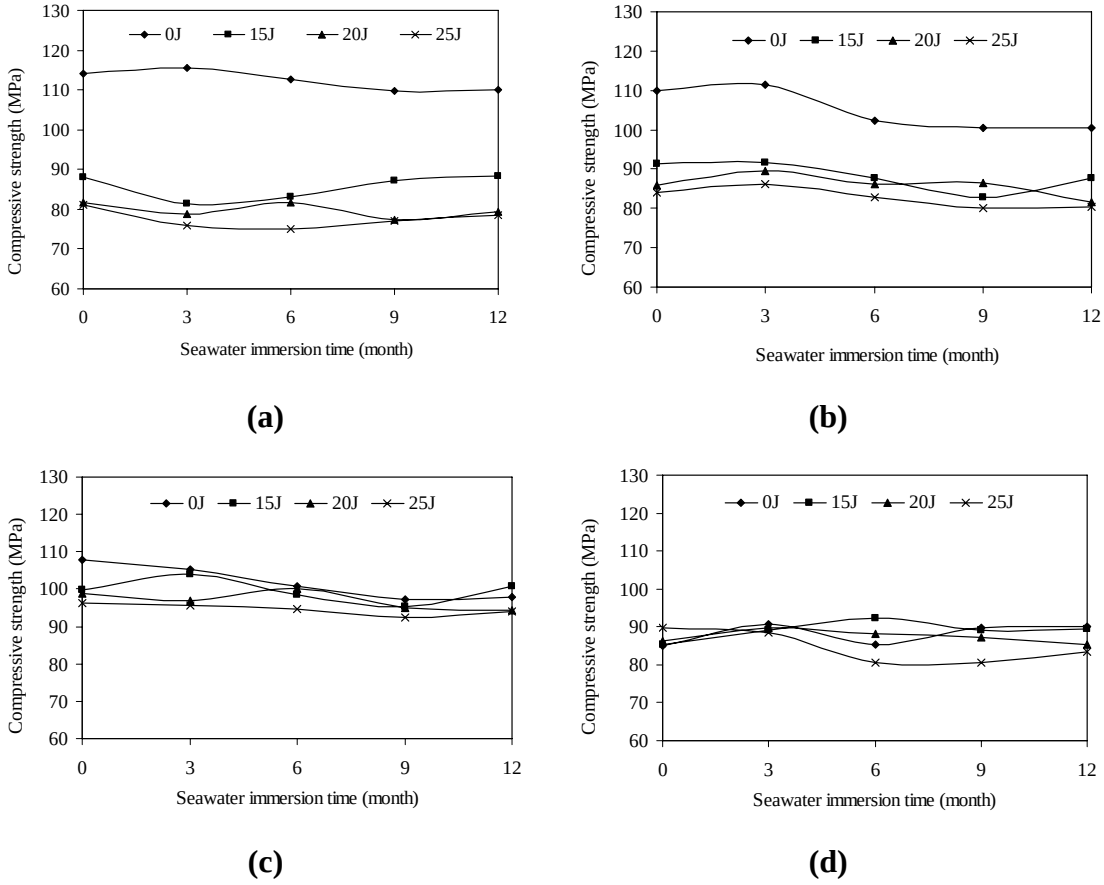

Figure 4.30 The compressive strength versus seawater immersion time for different impact energies at the specimens with the diameter **(a)** 50 mm, **(b)** 75 mm, **(c)** 100 mm, and **(d)** 150 mm

A composite specimen generally absorbs a certain amount of seawater. Salt water weakens the interface of epoxy and glass fiber. Therefore, for seawater exposure conditions decrease in impact resistance was observed. A similar trend of decrease was observed on the compressive strength.

CHAPTER FIVE
CONCLUSIONS AND RECOMMENDATIONS

The main objectives of the present study are to investigate the effect of environmental conditions on the transverse impact resistance and the compressive strength of the composite pipes with various diameters. E-Glass/epoxy composite pipes were manufactured by filament-winding method in the $[\pm 55^{o}]_3$ orientations. Compressive characteristics were obtained according to the seawater absorbing duration and the impact energies. Based on the results of this experimental study, the following conclusions can be drawn:

- The failure area decreases with increasing specimen diameter. Decreasing the diameter of the pipe increase the difference of the slope of its force-deflection curve.

- The incline section of the contact force-deflection curves consist of two slopes. Smaller difference between the slopes indicates the smaller damage. The pipes having larger diameter have this kind of curve.

- The impact characteristics of the pipe specimens having diameter-50 mm such as contact force, absorbed energy and maximum deflection are less affected by seawater.

- Third month of the seawater absorbing time is critical for all impact characteristics. The experiments performed at the end of third months show that the absorbed energy and maximum deflection values have the minimum values as the peak force has maximum.

- Impact behavior of 3-month seawater immersion specimens is different from the other environmental conditions specimen's behavior. The reason is that, 3-month specimens moisture weight gain (versus time of exposure) are less than the other

immersion times. Gained moisture by 3-month specimens due to absorb some impact energy these specimens are showed behavior that is more elastic. Because of this, contact time value higher than the other environmental conditions. Figure shows that 25J except contact force is less than the other results.

- For all of the specimen diameters contact force increases with increasing impact energy. For 50 mm diameter specimen contact force is less affected by seawater. However, on the other diameters, contact force reaches maximum value at 3-month after then generally tendency observed.

- Deflection values are important characteristics for evaluating an impact event effect for impact response of specimen pipes. For the all diameters, deflection values increase with increasing impact energy. Deflection is reverse ratio with contact force and so of in information about contact force reverse to deflection value due to seawater-immersed time.

- On specimen, it may be elastic strain energy due to different between impact energy and absorbed energy and this energy lead to rebounding of the impactor. In addition, absorbed energy decreases by increasing the diameters of specimen with elastic strain energy. For this reason, it shows that with the decrease in diameter of specimens become smoothly less flexible and the impact energy consumes by way of elastic deformations to a slight extent. Because of this, compared to the large diameter pattern, small diameter specimens also occur due to fiber breaking, increases absorbed energy value. It is clear that for 3-month the immersed specimens absorbed energy is less and not any important change (As can be seen from Figures). In addition, absorbed energy increases by increasing impact energy.

- In each environmental conditions and for every diameter specimen impact damage area increases by increasing impact energy. Flexibility of the specimens increase with increasing diameter of the specimen. Thus, damage size decreases

by increasing diameter. As a result, elastic strain energy is higher and absorbed energy value is lower. Therefore, impact damage area decreases with increasing specimen diameter.

- Failure of the specimen pipe with 50 mm diameter in circumferential direction is restrained by diameter. As a result of this, failure which extended in the longitudinal direction for the specimen pipe with 50 mm diameter is higher than that of 75 mm diameter.

- Compression-after impact strength increases with the increase with specimen pipe diameter, while it decreases with increasing of impact energy, except for the 150 mm diameter. But it does not change significantly in the largest diameter because of buckling.

- The compression-after impact damage propagates in the fiber direction of the pipe specimen with the smallest diameter. By increasing the specimen pipe diameter, damage generally extended in the circumferential direction from the point of impact. In the specimen pipe with the largest diameter, the damage mode is buckling. The damage does not start from point of impact or impact-induced damage.

Following are some of the recommendations for any future work to be carried out on composite pipes of the effect of environmental conditions and impact damages:

- The environmental such as humidity, ultraviolet radiation, and temperature effects on the impact response and compressive strength may be investigated.

- Accelerated water/seawater for higher time periods can be investigated to explain impact properties degradation of the composite pipes.

- The impact behavior and compressive strength of the different composite material types such as carbon/epoxy or kevlar/epoxy may be tested.

REFERENCES

Abrate, S. (1991). Impact on laminated composite materials. *Applied Mechanics Review, 44,* 155-190.

Abrate, S. (1994). Impact on laminated composites: Recent Advances. *Applied Mechanics Review, 47,* 517-544.

Abrate, S. (1998). *Impact on composite structures.* Cambridge: Cambridge University Press.

Aktas, M. (2007). *Temperature effect on impact behavior of laminated composite plates.* Ph.D Thesis, Dokuz Eylül University.

Atas, C. (2004). *Large deformations in composite laminated plates.* Ph.D Thesis, Dokuz Eylül University.

Cantwell, W.J., & Morton, J. (1991). The impact resistance of composite materials - a Review. *Composites, 22,* 347-362.

Changliang, Z., Mingfa, R., Wei, Z., & Haoran, C. (2006). Delamination prediction of composite filament wound vessel with metal liner under Low velocity impact. *Composite Structures,* 75, 387-392.

Chib, A. (2003). *Parametric study of low velocity impact analysis on composite tubes*. M.Sc Thesis, Wichita State University.

D'Almedia, J.R.M. (1991). Effects of distilled water and saline solution on the interlaminar shear strength of an aramid epoxy composite. *Composites, 22(6),* 448-450.

Deniz, M.E., Karakuzu, R., Sari, M., & Icten, B.M. (2010). Effects of seawater and transverse impact on axial compressive strength of glass/epoxy composite pipes. *13th International Materials Symposium (IMSP'2010),* 509-515.

Deniz, M.E., Karakuzu, R., Sari, M., & Icten, B.M. (2011). On the residual compressive strength of the glass-epoxy tubes subjected to transverse impact loading. *Journal of Composite Materials,* DOI: 10.1177/0021998311410483.

Doyum, A.B., & Altay, B. (1998). Detection of low-velocity impact damage in glass/epoxy tubes by penetrant method. *Insight*, 40(2), 117-121.

Doyum, A. B., & Altay, B. (1997). Low-velocity impact damage in glass fiber/epoxy cylindrical tubes. *Materials & Design, 18(3),* 131-135.

Estekanchi, H.E., & Vafai, A. (1999). On the buckling of cylindrical shells with through cracks under axial load. *Thin-Walled Structures, 35,* 255-274.

Gning, P.B., Tarfaoui, M., Collombet, F., Riou, L., & Davies, P. (2005). Damage development in thick composite tubes under impact loading and influence on implosion pressure. *Composites Part B: Engineering, 36 (4),* 306-318.

Gning, P.B., Tarfaoui, M., Collombet, F., & Davies, P. (2005). Prediction of damage in composite cylinders after impact. *Journal of Composite Materials, 39 (10),* 917-928.

Gong, S.W., Lam, K.Y., & Reddy, J.N. (1999). The elastic response of functionally graded cylindrical shells to low-velocity impact. *International Journal of Impact Engineering, 22*, 397-417.

Huang, J., Wang, X. (2009). Numerical and experimental investigations on the axial crushing response of composite tubes. *Composite Structures, 91,* 222-228.

Icten, B.M. (2006). *Damage in laminated composite plates subjected to low-velocity impact.* Ph.D Thesis, Dokuz Eylul University.

Imielinska K., & Guillaumat, L. (2004). The effect of water immersion ageing on low-velocity impact behaviour of woven aramid-glass fibre/epoxy composites. *Composites Science and Technology, 64*, 2271-2278.

Jiming, Z., & James P.L. (1994). The effects of a water environment on anomalous absorption behavior in graphite/epoxy composites. Department of Materials Science and Mechanics, Michigan State University, East Lansing, Michigan 48824, USA.

Joshi, S.P., & Sun, C.T. (1987). Impact-induced fracture initiation and detailed dynamic stress field in the vicinity of impact. *Proc. American Society of Composites 2nd Tech. Conf.* 177-185.

Khalid, A.A. (2001). Finite element and experimental analysis for the performance of hybrid composite tubes under crushing. *Pakistan Journal of Applied Sciences, 1(3),* 438-442.

Khalili, S.M.R., Soroush, M., Davar, A., & Rahmani, O. (2011). Finite element modeling of low-velocity impact on laminated composite plates and cylindrical shells. *Composite Structures, 93,* 1363-1375.

Kim, S.J., Goo, N.S., & Kim, T.W. (1997). The effect of curvature on the dynamic response and impact-induced damage in composite laminates. *Composites Science and Technology, 51,* 763-773.

Kistler, L.S., & Waas, A.M. (1998). Experiment and analysis on the response of curved laminated composite panels subjected to low velocity impact. *International Journal Impact Engineering, 21,* 711-736.

Kistler, L.S., & Waas, A.M. (1999). On the response of curved laminated panels subjected to transverse impact loads. *International Journal Solids Structures, 36,* 1311-1327.

Kootsookos, A., & Mouritz, A.P. (2004). Seawater durability of glass and carbon-polymer composites. *Composites Science and Technology, 64,* 1503-1511.

Krishnamurthy, K.S., Mahajan, P., & Mittal, R.K. (2003). Impact response and damage in laminated composite cylindrical shells. *Composite Structures, 59,* 15-36.

Liu, D. & Malvem, L.E. (1987). Matrix cracking in impacted glass/ epoxy plates. *Journal of Composite Materials, 21,* 594-609.

Liu, H.K., Tai, N.H., & Lee, W.H. (2002). Effect of seawater on compressive strength of concrete cylinders reinforced by non-adhesive wound hybrid polymer composites, *Composites Science and Technology, 62(16),* 2131-2141.

Mahdi, E., Hamouda, A.M.S., Sahari, B.B., & Khalid, Y.A. (2003). On the collapse of cotton/epoxy tubes under axial static loading. *Applied Composite Materials, 10,* 67-84.

Mallick, P.K. (1993). *Fiber-reinforced composites,* (2 rd edition). Marcel Dekker Inc., NewYork.

Mamalis, A.G., Manolakos, D.E., Ioannidis, M.B., & Papapostolou, D.P. (2006). The static and dynamic axial collapse of CFRP square tubes: Finite element modeling. *Composite Structures, 74,* 213-225.

Mantel, S.C., & Cohen, D. (2000). *Filament winding, International Processing of Composites*. Hanser.

Matemilola, S.A. & Stronge, W.J. (1997). Impact response of composite cylinders. *Int. Journal of Solids Structures, 34(21),* 2669-2684.

Naik, M.K. (2005). *The effect of environmental conditions on the hydrostatic burst pressure and impact performance of glass fiber reinforced thermoset pipes*. M.Sc Thesis, Kinh Fahd University of Petroleum & Minerals, Dhahran.

Palmer, A., Neilson, A., & Sivadasan, S. (2006). Pipe Perforation by medium-velocity impact. *International Journal of Impact Engineering, 32,* 1145-1157.

Palmer, A., Touhey, M., Holder, S., Anderson, M., & Booth, S. (2006). Full-scale impact tests on pipelines. *International Journal of Impact Engineering, 32,* 1267-1283.

Reddy, J. N. (1997). *Mechanics of laminated composite plates and shells: theory and analysis*. CRC Press, (Boca Raton, FL: Chemical Rubber Company).

Schultz, M.R. (1998). *Energy absorption capacity of graphite-epoxy composite tubes*. M.Sc Thesis, The Faculty of the Virginia Polytechnic Institute and State University.

Shivakumar, K.N., Elber, W., & Illg, W. (1985). Prediction of low-velocity impact damage in thin circular laminates. *A1AA Journal, 23,* 442-449.

Sjoblom, P.O., Hartness, J.T. & Cordell, T.M. (1988). On low velocity impact testing of composite materials. *Journal of Composite Materials, 22,* 30-52.

Soutis, C., & Turkmen, D. (1997). Moisture and temperature effects of the compressive failure of CFRP unidirectional laminates. *Journal of Composite Materials, 31(8),* 832-849.

Strait, L.H., Karasek, M.L., & Amateau, M.F. (1992). Effects of seawater immersion on the impact resistance of glass fiber reinforced epoxy composites. *Journal of Composite Materials, 26(14),* 2118-2133.

Tarfaoui, M., Gning, P.B., & Collombet, F. (2007). Residual strength of damaged glass/epoxy tubular structures. *Journal of Composite Materials, 41(18),* 2165-2182.

Tarfaoui, M., Gning, P.B., Davies, P., & Collombet, F. (2007). Scale and size effects on dynamic response and damage of glass/epoxy tubular structures. *Journal of Composite Materials, 41(5),* 547-558.

Tarfaoui, M., Gning, P.B., & Hamitouche, L. (2008). Dynamic response and damage modeling of Glass/Epoxy tubular structures: Numerical investigation. *Composites: Part A, 39*, 1-12.

Wu, L., Murphy, K., Karbhari, V.M., & Zhang, J.S. (2002). Short-term effects of sea water on E-glass/vinylester composites. *Journal of Applied Polymer Science, 84*, 2760-2767.

Xu, X., Ma J., Lim, C.W., & Chu, H. (2009). Dynamic local and global buckling of cylindrical shells under axial impact. *Engineering Structures, 31*, 1132-1140.

Yao, J. & Ziegmann, G. (2007). Water absorption behavior and its influence on properties of GRP pipe. *Journal of Composite Materials, 41*, 993-1008.

Zeng, T., Fang D., & Lu, T. (2005). Dynamic crashing and impact energy absorption of 3D braided composite tubes. *Material Letters, 59*, 1491-1496.

Zhang, M., & Mason, S.E. (1999). The effects of contamination on the mechanical properties of carbon fibre reinforced epoxy composite materials. *Journal of Composite Materials, 33*, 1363-1374.

Zhao, G., & Cho C. (2004). On impact damage of composite shells by a low-velocity projectile. *Journal of Composite Materials, 38(14)*, 1231-1254.

Zhou, J., Lucas, J.P. (1995). The effects of water environment on anomalous absorption behaviour in graphite/epoxy composites. *Composite Science and Technology*, 53, 57-64.